EXPLORING GLOBAL DYNAMICS IN A LOW ORDER MODEL OF PARALLEL SHEAR FLOW

By

Behzad Nikzad

A Thesis Submitted in Partial Fulfillment

of the Requirements for the Degree of

Master of Science

in

The Faculty of Science

Modelling and Computational Science

August 2015

Abstract

The study of the onset of turbulence in the flow of fluids, which are governed by the Navier-Stokes equations, has produced some famous instabilities e.g. Kelvin Helmholtz instability. An important, and as of yet mysterious, flow is Plane Couette flow in which turbulence is observable. Another observable phenomenon in Plane Couette flow is a "bursting" process whereby along with the linear laminar profile, non-laminar coherent structures appear and dissipate regularly. Yet, surprisingly V.A. Romanov has proven that the linear laminar profile of Plane Couette flow is linearly stable for all Reynolds number. In order to reconcile these seemingly contradictory facts a search began for numerical periodic solutions to Plane Couette flow. Nagata produced the first such solution and since then many others have been found as well. In order to explain the "bursting" process Fabian Waleffe introduced a low order model of Plane Couette flow that exhibits the phenomenon. We study the bifurcation diagram of a periodic solution of the Waleffe model found by the method of Nagata. Therein we find a co-dimension 2 bifurcation. The type of bifurcation, namely LPNS, ensures that we can find homoclinic and heteroclinic connections of limit cycles in the parameter space surrounding the it. We use a matrix-free manifold computation method to find a homoclinic orbit of limit cycles. Finally we will discuss a method to continue the homoclinic orbit.

Acknowledgements

I am grateful for the help and guidance of Prof. Lennaert van Veen. He introduced me to the wildly interesting world of bifurcation theory and turbulence in fluids. His dedication to the advancement of science in a cordial environment is inspirational and one that I wish to emulate. Without his patience and organized vision I would not have completed this thesis.

This thesis would not be possible without the support of my family. They have provided the shade under which I have worked all my life. My academic achievements are as much theirs as they are mine.

I would like to thank my friends. Those of you within the lab who made coming to work a joy and those of you who made my time away from work a joy. Social support is crucial for the completion of any task, especially one as stressful and arduous as the writing of a graduate thesis.

The faculty and staff of the Modeling and Computational Science department have been exceptional. I learned a lot of interesting things from incredible people. The jovial and friendly environment that the faculty foster should be celebrated.

To my companion and my cat: We did it!

For the mountains that bore me, the river that nurtured me, and the people that have suffered between them.

Contents

List of Figures

List of Tables

Introduction

1.1 Turbulence and Stability

This thesis is an exploration in the study of turbulence. The word turbulence conjures dramatic movement and complex indiscernible patterns. Frequent fliers are reminded of the feeling of unease felt when the pilot announces "we will be experiencing some turbulence". The avid student of the arts is perhaps reminded of the famous painting by Hokusai shown in Figure 1.1 below.

Figure 1.1: The Great Wave off Kanagawa. This picture is taken from [3]

.

The notion of turbulence is intuitive because we experience turbulence everyday. Examples of turbulence include the air passing by our cars as we drive to work, the motion of the smoke from our favourite hookah and the flow of water by a bridge pier in a lake. However, while this notion is intuitive it is not precise. A generally commonality between the examples given above is that medium within which turbulence

occurs are fluids i.e. substances which can change shape easily. We can make this definition more precise by introducing shear forces. A shear force is a force which pushes one part of a body in one direction while another part in a different direction. A fluid is then a substance which does not resist shear forces. For example liquids and gases are fluids while solids are not.

The flow of a fluid does not necessarily need to be turbulent. We do not perceive the perfectly still tea in the tea cup to be turbulent. Moreover we don't perceive the creep of maple syrup as it spreads over pancakes to be turbulent either. This means that we don't want to call all fluid motion turbulent . The non-turbulent flow of a fluid can be smooth and laminar i.e. the fluid flows in layers, with each layer maintaining its velocity. This occurs for example when water flows through a thin circular pipe (filling the pipe) at a slow speed. The fluid in this case flows in cylindrical layers centered around the pipe's axis of symmetry. The layers closer to the center moving faster and the layer in contact with the surface of the pipe not moving at all. This type of layered flow is called laminar flow.

In the example above (water flowing through a pipe) as the average speed of the water increases the laminar flow disappears and instead we observe turbulent flow. This is an example of a transition to turbulence from an orderly laminar profile. Over the last two centuries experimental and theoretical scientists have been looking for paradigms to explain the phenomenon of the onset of turbulence in generality. There is still no consensus on a definition of turbulence, however many concepts have been formalized in order to explain this transition.

Suppose we have a laminar flow in a specified geometry. Then the laminar flow is said to be Lyapunov stable if any small variations we add to the the laminar flow remain small as time goes on. The laminar flow is said to be asymptotically stable if any small variations we add dissipate over time. Finally we say that the laminar profile is linearly stable if any small variations we add dissipate over time at an expo-

nential rate. So that linear stability is encompassed by asymptotic stability which is itself encompassed by Lyapunov stability. Alternatively we say that a laminar profile is linearly unstable if there is at least one small perturbation that will grow exponentially over time. We also have the notions of global and local stability. As the names suggests a laminar flow is said to be locally stable if it is stable for a set of small perturbations and globally stable if it is stable for any perturbations.

Using these notions of stability we can describe the onset of turbulence. For example given a laminar flow in a specified geometry is linearly unstable, then small perturbations can grow and the laminar profile can dissipate. A concrete example of this is the flow of a fluid between two co-rotating cylinders which is called Taylor-Couette Flow (TCF). For a fluid with a given viscosity and for a fixed distance between the cylinders we can specify rotation speeds such that a laminar profile can persists even if we add small perturbations. However at other specified speeds then small perturbation will grow into a different type of flow known as Taylor Vortices. This is something which we can derive analytically, but is also observed experimentally [16]. At higher speeds we can even observe turbulence emerging from small perturbations in the laminar profile.

One approach to understanding turbulence has been to study the onset of turbulence in simple models. Models such as the flow of a fluid between co-rotating cylinders, the flow of a fluid through a cylindrical pipe, the flow of a fluid which is restricted between parallel plates, the flow a fluid between 2 parallel planes moving in opposite directions, etc. The general problem of finding criterion which can be used to decide the conditions under which laminar flow is replaced by turbulent flow has proven to be notoriously difficult, even for the simple models listed above. Any insight into these phenomenon could help us to actively create conditions under which transition to turbulence does occur or does not occur in more complex systems. This thesis is concerned with the simple system called Plane Couette Flow (PCF), which is the flow of a fluid between two infinite plates moving in opposite directions. A simple

laminar profile does exist for this system and it has been proven to be linearly stable. So the above approach does not work for PCF.

Another method of understanding turbulence in a system is by finding solutions and connecting orbits between them. That is turbulence can be described as the flow of a fluid as it meanders between orderly patterns of flow. If we had an exhaustive list of all equilibrium and all periodic solutions we could describe turbulence as a flow which spends time near some solution and then wanders off to shadow another solution and then another ad infinitum. While it is not likely that we can find such an exhaustive list, the exploration of these non-trivial solutions, and more importantly the connections between them would aid us in understanding turbulence. In fact many periodic solutions to PCF have been found [13]. Flows which connect periodic orbits have also been computed. Some of these connections are between one orbit and another and are called heteroclinic orbits [11]. Other connections are from a periodic orbit to itself [12], these are called homoclinic orbits. These connecting orbits are called heteroclinic orbits. This thesis aims to further that research.

1.2 Thesis Organization

In Chapter 1 we introduce the Navier-Stokes equations and discuss the notion of the onset of instability of simple laminar flows in basic geometries. PCF is introduced and the stability of laminar profile in PFC is presented in greater detail. We then present the work which has been done in finding non-trivial solutions to PCF and their relation to the study of the onset of turbulence in PCF. We then introduce Waleffe's low order model for PCF which we use for the remainder of the thesis.

Waleffe's low order model of PCF is a system of ODEs. This means that we can perform bifurcation analysis on the model. This forms the content of Chapter 2. We begin by introducing the basic notions required to rigorously talk about bifurcations including normal forms. We then present the LPNS bifurcation which is a co-dimension 2 bifurcation. We then present our results that were found using bifurcation analysis

using MatCont, specifically that an extended Waleffe model displays an LPNS bifurcation. We discuss the importance of this bifurcation in the study of the onset of turbulence.

The crux of the results for this thesis can be found in Chapter 3. Therein we present a homoclinic orbit for the extened Waleffe model found using a manifold computation method. We introduce the manifold computation method and present along with the homoclinic orbit other interesting results. Finally in Chapter 4 we present a method to continue the homoclinic orbit found in Chapter 3 and discuss the relevance of such a computation.

1.3 The Navier Stokes Equations

The flow of a fluid can be described by the Navier-Stokes (NS) equations:

$$\rho\left(\vec{u}_t + (\vec{u}\cdot\nabla)\,\vec{u}\right) = -\nabla p + \mu\Delta\vec{u} + \vec{F} \tag{1.3.1}$$

Where: ρ is the density of the fluid.

$\vec{u} = (u, v, w)$ represents the 3-components of the velocity field.

p is the pressure.

μ is the dynamic viscosity of the fluid.

$\vec{F} = (F_x, F_y, F_z)$ represents any body forces acting on the fluid.

We restrict ourselves to the flow of incompressible fluids, that is flows with which are divergence free:

$$\nabla\cdot\vec{u} = 0 \tag{1.3.2}$$

The Navier-Stokes equations (1.3.1) together with divergence free condition (1.3.2) form the incompressible Navier-Stokes equations.

A general analytic solution to the incompressible Navier-Stokes equations is currently not known. Further whether a general solutions exist at all is an open infamous Millennium Prize Problem [10]. The Millennium Prize Problems are 7 problems stated

by the Clay Mathematics Institute with a prize of $1,000,000 for a correct solution. As of now 6 of the 7 problems remain unsolved. Although a general solution to the Navier-Stokes equation is not known, luckily specific solutions do exist for many conditions. Examples of known solutions are the parabolic profile in TCF and the linear laminar profile in PCF, these will be discussed in sections 1.4.4 and 1.5 respectively. The latter is of special interest for us as the subject of our study is the stability (more interestingly the instability) of solutions to the Navier-Stokes equations under the specified boundary conditions of PCF.

It is common to see the Navier-Stokes equations written with the use of the total derivative (material derivative). The total derivative describes the rate of change of some quantity (in our case momentum) in a given material element as it flows through the medium. The total derivative of a quantity $y(\vec{x}, t)$ subject to a velocity field $\vec{u}$ is given by:

$$\frac{Dy}{Dt} = \frac{\partial y}{\partial t} + (\vec{u} \cdot \nabla) y$$

If we take the physical quantity to be momentum in each of the x, y, z directions, then the Navier-Stokes equations can be written in the form:

$$\rho \frac{D\vec{u}}{Dt} = -\nabla p + \mu \Delta \vec{u} + \vec{F}$$

The left hand side can now be viewed simply as the acceleration of a fluid parcel in a co-moving frame. The right hand side of the Navier-Stokes equations has two components: body forces represented by $\vec{F}$ and the divergence of the stress-tensor . The divergence of the stress tensor is separated into $-\nabla p$ and $\mu \Delta \vec{u}$, which represent the effects of pressure and viscosity respectively. The last term $\mu \Delta \vec{u}$ describes energy dissipation due to shear stresses for a viscous fluid, but that is not clear a priori. It is common to consider solutions of the Navier-Stokes equations in a rectangular prism, V, with periodic boundary conditions [10]. Consider the energy of a solution of the Navier-Stokes equations in a periodic rectangular prism with periodic boundary conditions, and no external pressure gradient or body force.

$$E = \rho \int_V \frac{1}{2} \|\mathbf{u}\|^2 \, dV$$

The rate of change of Energy with respect to time is then given by:

$$\begin{aligned} \frac{\partial E}{\partial t} &= \rho \frac{\partial}{\partial t} \int_V \frac{1}{2} \|\mathbf{u}\|^2 \\ &= \rho \int_V \mathbf{u}_t \cdot \mathbf{u} dV \end{aligned}$$

Since the flow satisfies the Navier-Stokes equation we can replace $\mathbf{u}_t$ in the above:

$$\frac{\partial E}{\partial t} = \int_V \left(-\rho \left(\mathbf{u} \cdot \nabla\right) \mathbf{u} - \nabla p + \mu \Delta \mathbf{u}\right) \cdot \mathbf{u} \, dV$$

We can rearrange this and separate terms to get:

$$\frac{\partial E}{\partial t} = \rho \int_V \left(\left(\mathbf{u} \cdot \nabla\right) \mathbf{u}\right) \cdot \mathbf{u} \, dV - \int_V \left(\nabla p\right) \cdot \mathbf{u} \, dV + \int_V \left(\mu \Delta \mathbf{u}\right) \cdot \mathbf{u} \, dV$$

Now we consider each of the terms individually.

$$\begin{aligned} \int_V \left(\left(\mathbf{u} \cdot \nabla\right) \mathbf{u}\right) \cdot \mathbf{u} \, dV &= \int_V \left(\left(\nabla \times \mathbf{u}\right) \times \mathbf{u}\right) \cdot \mathbf{u} \, dV + \int_V \left(\nabla \left(\frac{1}{2} \|\mathbf{u}\|^2\right)\right) \cdot \mathbf{u} \, dV \\ &= \int_V \left(\nabla \left(\frac{1}{2} \|\mathbf{u}\|^2\right)\right) \cdot \mathbf{u} \, dV \end{aligned}$$

The last inequality follows from the fact that $\mathbf{u}$ and $(\nabla \times \mathbf{u}) \times \mathbf{u}$ are perpendicular. Then:

$$\begin{aligned} \int_V \left(\nabla \left(\frac{1}{2} \|\mathbf{u}\|^2\right)\right) \cdot \mathbf{u} \, dV &= \int_V \nabla \cdot \left(\frac{1}{2} \|\mathbf{u}\|^2 \mathbf{u}\right) \, dV - \int_V \left(\frac{1}{2} \|\mathbf{u}\|^2\right) \left(\nabla \cdot \mathbf{u}\right) \, dV \\ &= \int_V \nabla \cdot \left(\frac{1}{2} \|\mathbf{u}\|^2 \mathbf{u}\right) \, dV, \qquad \text{since } \nabla \cdot \mathbf{u} = 0 \\ &= \oint_S \left(\frac{1}{2} \|\mathbf{u}\|^2 \mathbf{u}\right) \cdot \mathbf{n} \, dS \\ &= 0 \end{aligned}$$

The last equality follows because we have periodic boundary conditions. It is interesting to note that this term vanishes at material boundaries as well as periodic

boundaries. We also have the following simplification:

$$\begin{aligned}\int_V (\nabla p)\cdot\mathbf{u}\ dV &= \int_V \nabla\cdot\left(p\mathbf{u}\right)\ dV - \int_V p\left(\nabla\cdot\mathbf{u}\right)\ dV \\ &= \int_V \nabla\cdot\left(p\mathbf{u}\right)\ dV, \qquad\qquad \text{since } \nabla\cdot\mathbf{u}=0 \\ &= \oint_S \left(p\mathbf{u}\right)\cdot\mathbf{n}\ dS \\ &= 0\end{aligned}$$

The last equality follows because we have periodic boundary conditions and there is no external pressure gradient. Write $\vec{u} := (u_1, u_2, u_3)$, then the rate of change energy has been simplified to:

$$\begin{aligned}\frac{\partial E}{\partial t} &= \mu\int_V (\Delta\mathbf{u})\cdot\mathbf{u}\ dV \\ &= \mu\sum_{i=1}^{3}\int_V (\Delta u_i)\,u_i\ dV \\ &= \mu\sum_{i=1}^{3}\int_V (\nabla\cdot(\nabla u_i))\,u_i\ dV \\ &= \mu\sum_{i=1}^{3}\left(\int_V \nabla\cdot(u_i\nabla u_i)\ dV - \int_V (\nabla u_i)\cdot(\Delta u_i)\ dV\right) \\ &= \mu\sum_{i=1}^{3}\int_V \nabla\cdot(u_i\nabla u_i)\ dV - \mu\sum_{i=1}^{3}\int_V (\nabla u_i)\cdot(\nabla u_i)\ dV \\ &= -\mu\sum_{i=1}^{3}\int_V \|\nabla u_i\|^2\ dV\end{aligned}$$

It is now readily observable that if no body forces or pressure gradients are present the energy of the system will tend to zero with increasing time.

It is also common to see the NS equations written in the form:

$$\vec{u}_t + (\vec{u}\cdot\nabla)\,\vec{u} = -\frac{1}{\rho}\nabla p + \nu\Delta\vec{u} + \vec{F}$$

Where $\nu = \mu/\rho$ is the kinematic viscosity of the fluid. Given a characteristic length, H, and a characteristic velocity, $\bar{U}$, then we can non-dimensionalize the Navier-Stokes

equations using the transformations:

$$\tilde{x} = \frac{1}{H}x \qquad \tilde{y} = \frac{1}{H}y \qquad \tilde{z} = \frac{1}{H}z \qquad \tilde{\vec{u}} = \frac{1}{\overline{U}}\vec{u} \qquad \tilde{t} = \frac{\overline{U}}{H}t$$

Then the non-dimensionalized Navier-Stokes, with the tilde notation dropped, are:

$$\begin{gathered}\left(\frac{\partial}{\partial t} - \frac{1}{Re}\nabla^2\right)\vec{u} = -\vec{u}\cdot\nabla\vec{u} - \frac{1}{\rho}\nabla p \\ \nabla\cdot\vec{u} = 0\end{gathered} \tag{1.3.3}$$

.

With Reynolds number $Re = \overline{U}H/\nu$. The Reynolds number is very important in the study of stability of solutions of the Navier-Stokes equations. Generally high Reynolds numbers are associated with more turbulent motion and low Reynolds number is associated with less complicated motions. For low Reynolds numbers we observe 'layers' of constant velocity where the shape of the layers emulate the geometry of the experiment. For example in the flow of a fluid in a pipe we observe cylindrical layers of constant velocity. Such 'layered' flows are called laminar profiles and explicit examples are given in section 1.4.

Another useful formulation of the Navier-Stokes equations is the vorticity equation. By taking the curl of (1.3.1) we find the vorticity equation:

$$\rho\left(\omega_t + (\vec{u}\cdot\nabla)\,\vec{\omega} - (\vec{\omega}\cdot\nabla)\,\vec{u}\right) = \mu\Delta\omega + \nabla\times\vec{F}$$

Alternatively:

$$\frac{D\omega}{Dt} = (\vec{\omega}\cdot\nabla)\,\vec{u} + \nu\Delta\omega + \nabla\times\vec{F} \tag{1.3.4}$$

Pressure is a scalar function and hence the curl of its gradient is zero.

An important tool for the study of solutions to the Navier-Stokes equations is the Poloidal-Toroidal decomposition. This is similar to the Helmholtz decomposition since the vector field is decomposed into two 'special' components. The Helmholtz decomposition allows us to write any vector field as a sum of its irrotational and divergence free components. In the case of incompressible fluids, $\nabla\cdot\vec{u} = 0$, then

we can further decompose the divergence free vector field into Toroidal and Poloidal components respectively as follows:

$$\vec{u} = \nabla \times \Psi\hat{e} + \nabla \times (\nabla \times \Phi\hat{e}) \tag{1.3.5}$$

where Ψ and Φ are scalar functions and $\hat{e}$ is a chosen unit vector. The Toroidal component represents vortical motion with $\hat{r}$ as the axis of symmetry. The Poloidal component does not have an easy geometrical representation. However if one imagines a very small magnet at the origin, then the Poloidal component is along the magnetic field lines as shown in Figure 1.2.

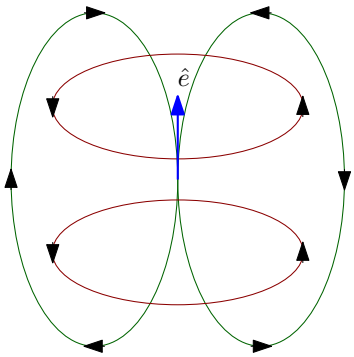

Figure 1.2: The blue arrow is the chosen vector $\hat{e}$, the brown lines represent the Toroidal component, and the green lines represent the Poloidal component.

1.4 Laminar Profiles in Simple Geometries

The following are examples of solutions to the Navier-Stokes equations under specified boundary conditions and geometries. For each example we are interested in the stability of the solution. We employ color coding and symbols to show the different boundary conditions and geometries. Forces will be drawn as red arrows, moving boundary conditions will be drawn as green arrows, stationary boundary conditions will be drawn as a dashed green line and the vector field of the fluid flow will be drawn as blue arrows. .

1.4.1 Plane Poiseuille Flow

PPF is the flow of a fluid between two infinite parallel plates forced by a pressure gradient across the channel. The fluid velocity at the plates is zero due to no-slip

boundary conditions. Suppose also that the pressure gradient is constant. A simple laminar profile solution to PPF (Figure 1.3) is parabolic flow under the following assumptions: :

$$\frac{\partial p}{\partial x} = P \quad , \quad \frac{\partial \vec{u}}{\partial t} = \vec{0} \quad , \quad v \equiv w \equiv 0 \implies \frac{\partial u}{\partial x} \equiv 0$$

The parabolic laminar profile solution is then given by:

$$\vec{u} = \left(\frac{P}{4\mu}(H^2 - y^2), 0, 0 \right) \tag{1.4.1}$$

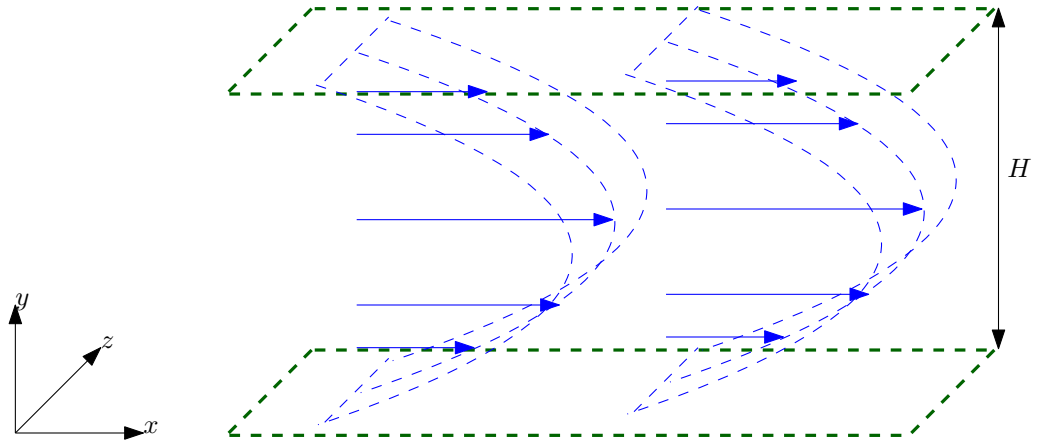

Figure 1.3: The laminar profile in PPF

This laminar profile is a valid solution for any value of Re. For small Reynolds number we observe this profile experimentally, however as we increase the Reynolds number in experiments and simulations the profile becomes unstable. The stability of PPF was studied by Heisenberg (better known for other work) using the Poloidal-Toroidal decomposition (1.3.5) of the Navier Stokes equations. He proved that the flow becomes unstable for $Re \simeq 5772$ [26]. Here the characteristic length is the width of the channel and the characteristic velocity is the mean velocity of the profile.

1.4.2 Pipe Flow

Pipe flow is the flow of a fluid inside of an infinite circular cylinder across the channel. A simple laminar profile to pipe flow shown in Figure 1.4. As in the case of PPF the laminar profile is parabolic. The parabolic laminar profile solution in cylindrical coordinates $\vec{u} = (u_r, u_\theta, u_z)$ is given by:

$$\vec{u} = \left(0, 0, \frac{P}{4\mu}(R^2 - r^2)\right) \tag{1.4.2}$$

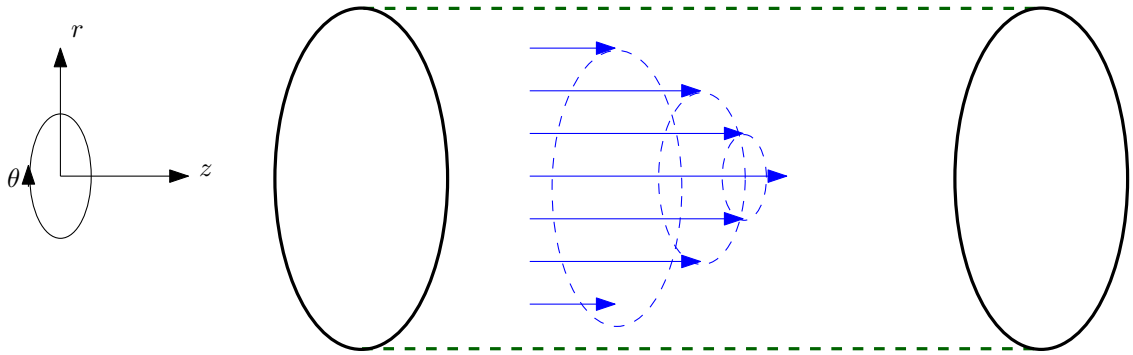

Figure 1.4: The laminar profile in Pipe Flow

Where R is the radius of the pipe. The characteristic length is the pipe diameter and the characteristic velocity is the mean velocity of the profile. This laminar profile is also a valid solution for any value of Re. Attempts to look for an instability for the parabolic laminar profile in pipe flow have been unsuccessful. In fact it is believed that the parabolic profile is stable for all Reynolds numbers. The stability of the parabolic profile has been shown experimentally for upto $Re \simeq 10^5$ [26].

1.4.3 Boundary Layer

Boundary layers occur when a fluid flows on a fixed plane. The fluid has zero velocity on the plane (no slip boundary conditions) and constant velocity, U, far away from the it. For low Reynolds number again we observe an laminar profile (Figure 1.5) which we can approximate with $\vec{u} = (u, 0, 0)$, with:

$$u = \begin{cases} U\left(1 - \dfrac{(z-H)^2}{H^2}\right) & \text{for } y \leq H \\ U & \text{for } y > H \end{cases} \tag{1.4.3}$$

Where H, the characteristic height is generally taken to be the distance from the plane at which the fluid velocity is $0.99U$. The characteristic velocity is taken to be U. Walter Tollmien and Hermann Schlichting proved that a 2D linear instability exists

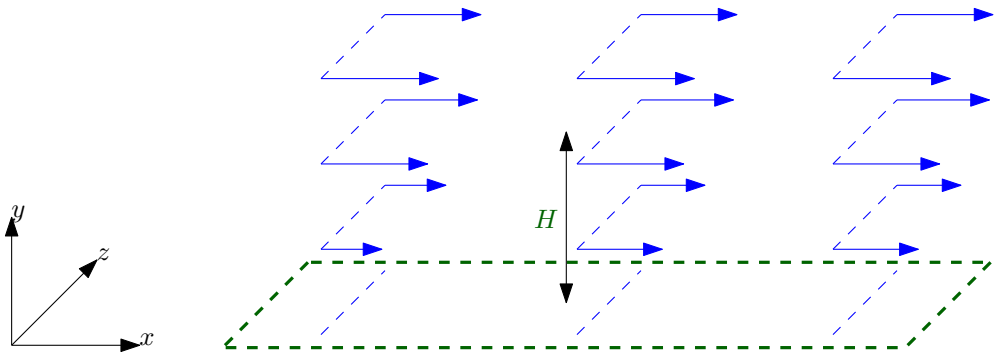

Figure 1.5: The laminar profile in boundary layers

for $Re \simeq 500$ [26].

1.4.4 Taylor-Couette Flow

TCF is the flow of a fluid between two co-rotating infinite cylinders as shown in Figure 1.6. Let R_1, R_2 be the radii and Ω_1, Ω_2 the angular velocities of the inner and outer cylinders respectively.

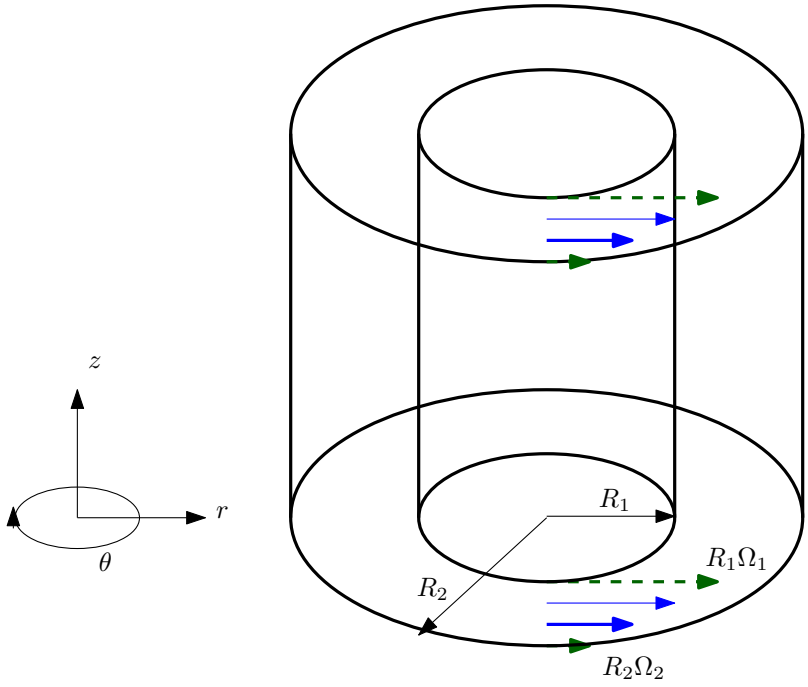

Figure 1.6: The laminar profile in TCF

A solution is the linear laminar profile $\vec{u} = (0, u_\theta, 0)$, such that

$$\begin{aligned} u_\theta &= Ar + \frac{B}{r} \\ &= \frac{\Omega_2 R_2^2 - \Omega_1 R_1^2}{R_2^2 - R_1^2} r + \frac{(\Omega_2 - \Omega_1) R_2^2 R_1^2}{R_2^2 - R_1^2} \frac{1}{r} \end{aligned}$$

We assume that:

$$\frac{\Omega_2 - \Omega_1}{\Omega_2} \ll 1 \qquad \text{and} \qquad \frac{R_2 - R_1}{R_2} \ll 1$$

The characteristic velocity, height and Reynolds number respectively are given by:

$$U = (\Omega_2 - \Omega_1) \frac{R_2 + R_1}{2} \quad , \quad H = R_2 - R_1 \quad , \quad Re = \frac{(\Omega_2 - \Omega_1)(R_2^2 - R_1^2)}{2\nu}$$

In the case of Taylor Couette flow there are two other dimensionless numbers which are important. The first, Ω, represents the Coriolis effect and is given by:

$$\Omega = \frac{(\Omega_2 + \Omega_1)(R_2 - R_1)^2}{\nu}$$

The second dimensionless number is, $T = \Omega(Re - \Omega)$, the Taylor number. It is a measure of the ratio of the energy input to dissipation. Geoffrey Taylor showed that the laminar profile becomes unstable for $T \simeq 1708$ and 'Taylor-Couette vortices' will form and grow exponentially thereafter [1]. Due to the effects of non-linear terms the 'Taylor-Couette vortices' become unsteady which then lead to 'wavy Taylor vortices' and finally turbulence [16].

1.4.5 Rayleigh-Bénard Convection

A closely related set up to TCF, though this is not clear a priori, is Rayleigh-Bénard Convection. In order to account for thermal effects, we use the Oberbeck-Boussinesq equations. These equations are an approximation of Navier-Stokes equations that include thermal effects. We find analytically an instability of a laminar solution to these equations. Consider a fluid which is differentially heated:

Suppose that the fluid can move freely at the plates and that the temperature is given by $T(x, y, z)$ as shown in 1.7. Suppose the plates are separated by a distance H which we use to non-dimensionalize space. Then $T_0(x, y, z) = (1 - y/H) T_2 + (y/H) T_1$ along with $\vec{u} = \vec{0}$ is a laminar solution. Consider now a perturbation of this solution

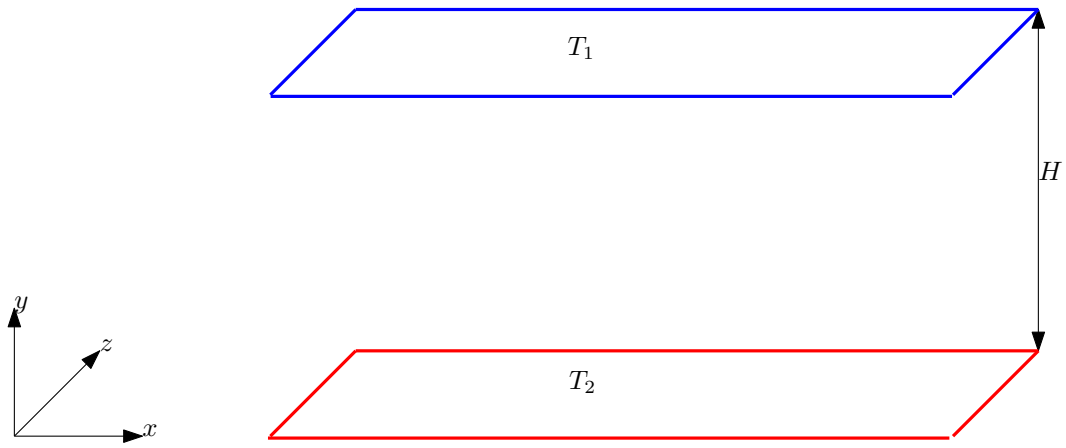

Figure 1.7: The setup of Rayleigh-Bénard convection. The top and bottom plates are kept at temperature T_1 and T_2 respectively.

with the temperature at the plates fixed. We choose the following perturbation from the linear gradient as:

$$T(x,y,t) = T_0 + \theta \quad , \quad \vec{u} = \vec{0} + (u, 0, w)$$

The divergence free condition then allows us define a stream function ψ such that:

$$u = \frac{\partial \psi}{\partial y} \qquad \text{and} \qquad w = \frac{\partial \psi}{\partial x}$$

This gives us $\nabla \times \vec{u} = \omega = \nabla^2 \psi$. The Oberbeck-Boussinesq equations can then be written in non-dimensionalized form as follows:

$$\nabla^2 \frac{\partial \psi}{\partial t} + \frac{\partial(\psi, \nabla^2 \psi)}{\partial(x,y)} - \sigma \frac{\partial \theta}{\partial x} - \sigma \nabla^4 \psi = 0$$
$$\frac{\partial \theta}{\partial t} + \frac{\partial(\psi, \theta)}{\partial(x,y)} - R \frac{\partial \psi}{\partial x} - \nabla^2 \theta = 0$$

We have used two dimensionless numbers σ the Prandtl number and R the Rayleigh Number. They are given by:

$$\sigma = \frac{\nu}{\kappa} \qquad\qquad R = \frac{g \epsilon H^3 (T_2 - T_1)}{\kappa \nu}$$

Where κ is the coefficient of thermal diffusivity, g is acceleration due to gravity, and ϵ is the coefficient of volume expansion. Consider only the linear terms of the system:

$$\nabla^2 \frac{\partial \psi}{\partial t} - \sigma \frac{\partial \theta}{\partial x} - \sigma \nabla^4 \psi = 0 \tag{1.4.4}$$

$$\frac{\partial \theta}{\partial t} - R \frac{\partial \psi}{\partial x} - \nabla^2 \theta = 0 \tag{1.4.5}$$

We consider solutions of the form $\psi = e^{\lambda t + i\gamma k x + i(q\pi)y}$ with $\lambda \in \mathbb{R}$ and $k, q \in \mathbb{Z}$ and $\gamma \in \mathbb{R}^+$. Here γ represents the aspect ratio of the wavelengths (of the same wavenumber) in the horizontal and vertical directions. The choice of ψ is not arbitrary, we are looking for solutions which are eigen-functions of the operators ∇^4 and $\nabla^2 \partial_t$. Then (1.4.4) and (1.4.5) become:

$$\lambda \left((\gamma k)^2 + (q\pi)^2 \right) \psi = -\sigma \frac{\partial \theta}{\partial x} - \sigma ((\gamma k)^2 + (q\pi)^2)^2 \psi = 0$$

$$\lambda \theta = i \left(\gamma k \right) \left(R \right) \psi - (k^2 + q^2) \theta$$

For convenience we write $(\gamma k)^2 + (q\pi)^2 = A$. Now we have a simple system of equations:

$$\begin{bmatrix} -\sigma A & -\frac{\sigma}{A} \left(i \left(\gamma k \right) \right) \\ i \left(\gamma k \right) \left(R \right) & -A \end{bmatrix} \begin{bmatrix} \psi \\ \theta \end{bmatrix} = \lambda \begin{bmatrix} \psi \\ \theta \end{bmatrix}$$

Now we compute the eigenvalues directly:

$$\lambda = \frac{-A(\sigma + 1) \pm \sqrt{(A(\sigma+1))^2 - 4 \left(\sigma A^2 - \frac{\sigma}{A} \left(\gamma k \right)^2 R \right)}}{2}$$

Taking the larger eigenvalue, we find

$$\lambda > 0 \quad \text{iff} \quad \sigma A^2 - \frac{\sigma}{A} \left(\gamma k \right)^2 R < 0 \quad \text{iff} \quad R > \frac{A^3}{\left(\gamma k \right)^2} = \frac{((\gamma k)^2 + (q\pi)^2)^3}{\left(\gamma k \right)^2}$$

It is obvious that for any fixed $\gamma \in \mathbb{R}$, then R has a minimum for $k = 1 = q$. Therefore we fix $k = 1 = q$, and using elementary calculus we find the minimum value of R as a function of γ. The minimum value is $R_{\text{crit}} = 27\pi^4/4$ which occurs at $\gamma_{\text{crit}} = \pi/\sqrt{2}$. .

This shows that the linear temperature gradient solution, under suitable assumptions, has a linear instability. This result was first shown by Rayleigh and is explained in [1] (page 311) and further discussion of the model developed by Saltzman can be found in [18]. It is of special historical interest to chaos theorists because it was used by Edward Lorenz as a model of atmospheric convection. Edward Lorenz's work with this model led to one of the earliest papers on chaos theory.

We mentioned earlier that Rayleigh Bénard convection is related to Taylor-Coutte flow. If we set no-slip boundary conditions, instead of free-slip boundary conditions as above, then the instability will occur at $R \simeq 1708$. This is not a coincidence, the equations which describe the two set ups are the same. [1].

1.5 Plane Couette Flow

The geometry of interest in this thesis is PCF shown in Figure 1.8. This is the flow of a fluid between two infinite plates which move in opposite directions at uniform velocity.

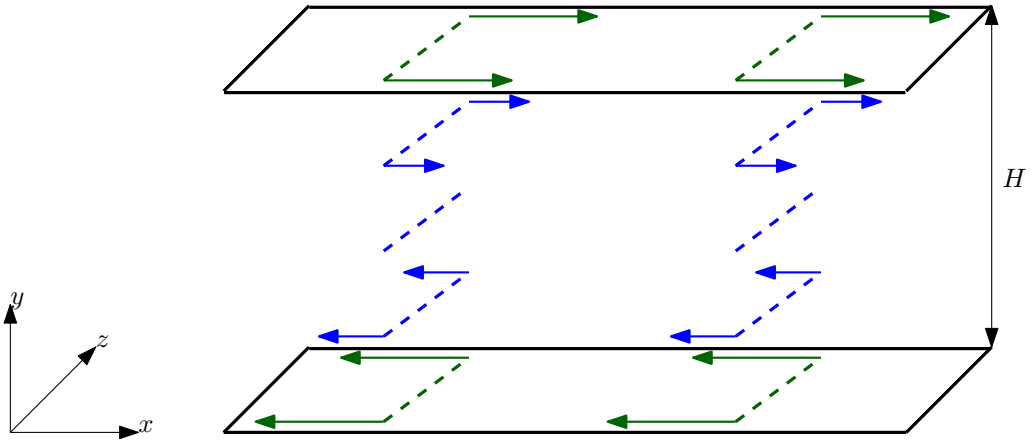

Figure 1.8: The laminar profile of the PCF

Henceforth we will also make reference to the streamwise, wall-normal and spanswise directions which will represent the flow in the x, y, and z directions.

The solution is again a linear laminar profile. The characteristic velocity is the plate velocity U and the characteristic length is the separation, H, between the plates.

The linear laminar profile is *linearly stable for all Reynolds numbers.* [17]. This is not a trivial result and was proven four decades ago. That is contemporary work by pure mathematics standards.

Romanov's result is one of functional analysis. Let $\Omega = \{x, y, z; |x| \leq 1, y, z \in \mathbb{R}\}$, then $v_0 = (0, 0, x)$ is the linear laminar profile solution to PCF. Consider a perturbation ν from v_0, then the non-dimensionalized Navier-Stokes equations for PCF can be written as:

$$\vec{\nu}_t = \frac{1}{Re}\Delta\vec{\nu} - (v_0 \cdot \nabla)\,\vec{\nu} - (\vec{\nu} \cdot \nabla)\,v_0 - \nabla p - (\vec{\nu} \cdot \nabla)\,\vec{\nu}$$
$$\nabla \cdot \vec{\nu} = 0 \quad , \quad \vec{\nu}|_{\partial\Omega} = \vec{0} \quad , \quad \vec{u}|_t = 0 = \vec{u_0}$$

We can write the system of differential equations as:

$$\vec{\nu}_t = A\nu + f\,(\nu)$$

Romanov establishes the asymptotic stability of v_0 by showing that the real part of all the eigenvalues of the operator A are negative for some open neighborhood of v_0. That is given any Reynolds number, then we can specify a domain of solutions that are close to the laminar profile which asymptotically converge to it. It is interesting to note that in Romanov's proof the rate of convergence of a perturbed solution is inversely proportional to the Reynolds number. That is the guaranteed rate of convergence of perturbed solutions with lower Reynolds number is higher than those of perturbed solutions with higher Reynolds number. This agrees with our intuition that at low Reynolds number any perturbation from the laminar profile should quickly dissipate.

The stability of the linear laminar profile in PCF is surprising from an experimental point of view. For Reynolds numbers between $Re \simeq 100$ and $Re \simeq 500$ the linear laminar profile is observed to break down and reform. The process of the breakdown of the laminar profile and its reformation is commonly referred to as the 'bursting' phenomenon [9]. For higher Reynolds number we observe turbulent motion. To rec-

oncile these experimental observations and the theoretical result of Romanov we note that they are not mutually exclusive. While Romanov's proof does show that at lower Reynolds number any perturbation in the specified open neighborhood would dissipate at a faster rate, it does not state the size or shape of the open neighborhood for which it is valid. That is to say that for any given Reynolds number the neighborhood in which any perturbation will dissipate could be smaller or larger than experimental tolerance. In any real world experiment we expect to have unwanted perturbations. These perturbation can be outside of the neighborhood for which linear stability applies. It stands to reason that the size of the neighborhood for which perturbations dissipate exponentially is larger for low Reynolds number and smaller for higher Reynolds number. This is because for low Reynolds number ($Re < 100$) we observe exponentially dissipation for small perturbations and for larger Reynolds number we observe the 'bursting phenomenon'.

One approach to this is by considering the normality of the operator associated with PCF. It is shown in [2] that the operator associated with a low order model of PCF is non-normal. Therein it is argued that this non-normality can cause transient growth of perturbations and hence a "bootstrapping" of experimental perturbations can lead to turbulence. So that perturbations from the linear laminar profile can excite more complex flows after which they may dissipate and the linear profile re-emerges. . On the other hand the operator associated with TCF is normal [19]. This perhaps explains the correspondence between linear stability theory and experimental results in TCF and the lack thereof in PCF [19]. However this approach has been criticized as not being fundamental to the transition to turbulence. Specifically Waleffe comments about these transient growths that "... the most amplified disturbances are streamwise independent and those can not trigger nonlinear effects that will prevent the eventual viscous decay" [24].

1.5.1 Coherent Structures and The SSP

A further observation is that certain coherent structures such as 'rolls' and 'streaks' reoccur in experiments, this suggests that perhaps there are simple solutions other

than the laminar profile to the Navier-Stokes equations in PCF.

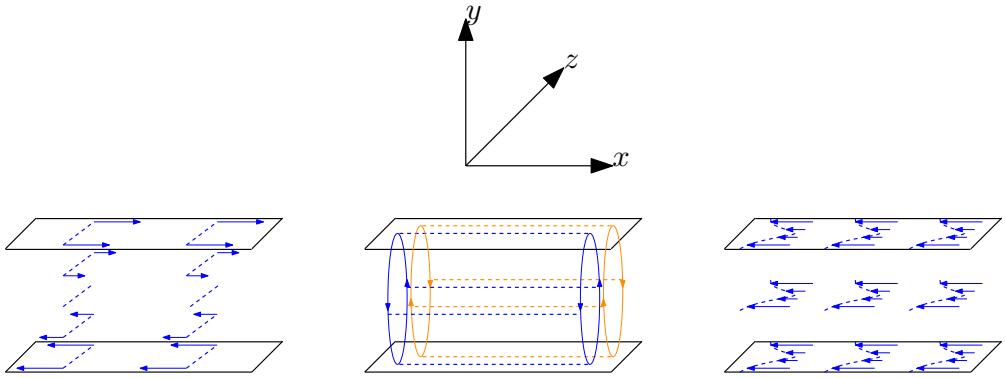

(a) The laminar profile (b) Roll (c) Streak

Figure 1.9: Examples of coherent structures

Recall that the TCF has a linear laminar profile which becomes unstable and morphs into the 'Taylor-vortex' flow. We observe the formation of analogous rolls experimentally in PCF. The axis of symmetry of these rolls is the stream wise direction in both geometries. These rolls transfer linear momentum (angular momentum) between the differentially moving plates (cylinders) thereby creating 'streaks' in PCF (TCF). 'Streaks' refer to fluid streaks which flow from one plate to the other carrying with them their momentum.

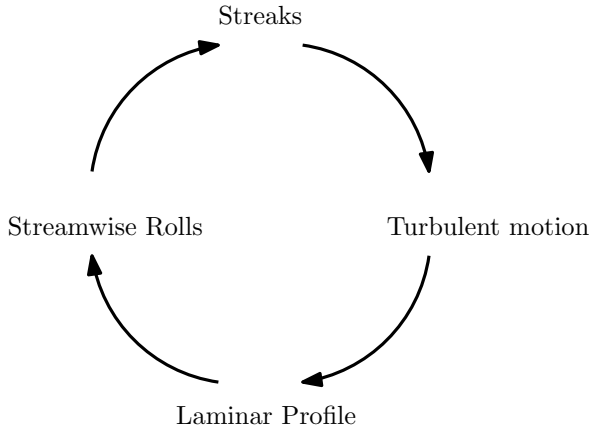

Figure 1.10: The SSP process as described by Waleffe

For TCF the 'Taylor-vortex' flow is seen to be experimentally stable. In the case of PCF, the streaks stimulate turbulence, and after a period of turbulence the laminar

profile reforms. For low Reynolds number rolls and turbulence occur for a very short period within the cycle. The fluid appears to burst hence giving rise to the name of the phenomenon [9]. This suggests that there might be non-trivial non-laminar solutions to PCF which are nevertheless coherent, i.e. 'streaks', 'rolls'. . Such non-laminar solutions to PCF, if found, would give us insight into the turbulence observed in PCF. .

Nagata attempted to find such non-laminar solutions. He found the first non-trivial solution to the PCF, namely a travelling wave solution. The method which Nagata used to find the travelling wave solution is of interest to us. TCF, which is the flow of a fluid trapped between two differentially rotated infinite cylinders, has a laminar profile solution like PCF. Another solution of the Taylor-Couette flow is the Taylor-Vortex solution. This solution can be found by continuation methods which will be discussed in Chapter 2. Nagata posed the problem by using the Poloidal-Toroidal decomposition and numerically representing the quantities by their expansion using Fourier basis functions. By using truncated Fourier expansions he numerically computed the Taylor-Vortex solution and then reduced Ω (defined in Section 1.4.4) to zero. The equations describing TCF are precisely those describing PCF if Ω is zero [16] . This is a homotopy continuation of a periodic solution within TCF into one of PCF. In order to ensure that this is not a computational artifact Nagata computed the solution for many different truncation levels and showed that the results were very similar. The resulting non-trivial solution is a steady solution which has an upper branch and lower branch for Reynolds number above a certain value which depends on the aspect ratios. It is believed that this solution exhibits a 'bifurcation from infinity'. That is the two branches remain separated as the Reynolds number is increased.

Kawahara and Kida found two periodic solutions for PCF [11]. The first solution is a standing wave which goes back and forth between two solutions of Nagata's. Those two solutions are in fact equivalent through translations by half the streamwise length. The second solution has high temporal and spatial variation. Unlike previous solutions, which were simple, this solution exhibits the SSP process. That is we can

see the formation of streamwise vortices which are replaced by streaks followed by turbulence and the regeneration of the streamwise vortices.

In Figure 1.11 the solutions are projected onto the 2D plane consisting of the energy dissipation rate and the energy input rate. This is called the projection on the (I,D)-plane. Kawahara and Kida compute two turbulent solutions which connect their periodic solutions on the (I,D)-plane. This suggests that there are orbits which begin near one periodic solution and overtime meander to the other periodic solution, i.e. a heteroclinic orbit.

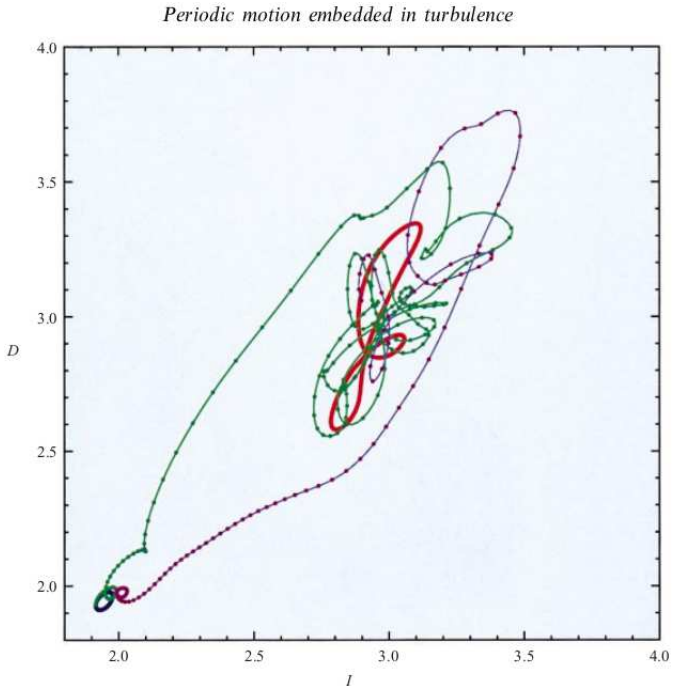

Figure 1.11: The blue and red trajectories represent the the two periodic solutions. The green (purple) trajectory represents a seemingly heteroclinic orbit from the blue (red) orbit to the red (blue) orbit. This graph is taken from [11].

The second solution is also remarkable from a historic point of view. Kawahara and Kida also found a turbulent solution which shadows the periodic solution. The two solutions have near identical mean velocities and root-mean-square velocities. The projection of the periodic and the turbulent solution onto the (I,D)-plane shows the

turbulent solution staying close to the periodic solution with occasional escapes. This was the first time a periodic solution which is shadowed by a turbulent one had been numerically demonstrated in PCF and in general. Recall that heteroclinic orbits and the shadowing of non-trivial solutions was a proposed as a possible explanation of turbulence in our introduction.

The results of Kawahara and Kida were extended by Viswanath, who performed computationally intensive calculations to find six more periodic solutions, one steady and five periodic [22]. The computations approximated solutions of PCF using a mix of Fourier functions (streamwise-spanwise directions) and Chebyshev functions (wall-normal direction). Viswanath's computations conclusively showed that these non-trivial solutions are not numerical artifacts and in fact solutions to the NS equations. He computed the energy spectra of the periodic solutions and found a clear convergence to zero as the wave number increased in any of the three directions . He further solidified the validity of the solutions by recomputing the solutions at higher resolutions and then computing the relative error. .

1.5.2 The Low Order Model

Recall that PCF was the flow of a fluid between two infinite plates moving with equal and opposite velocity with no-slip boundary conditions as shown in Figure 1.8. Computations of solutions to PCF are normally done using Fourier modes in the streamwsie and the spanwise directions and Chebyshev polynomials in the wall-normal direction as in [22]. The reason Chebyshev polynomials are used in the wall-normal direction is that PCF has fixed boundary conditions in the wall-normal direction. If we use fourier modes in the wall-normal direction this would lead to computational artificats such as the Gibbs phenomonon.

Fabian Waleffe created a low order model of a set up similar to PCF shown in Figure 1.12, which has many of the interesting properties of PCF. It is not impossible to create a low-order model of PCF which uses Chebyshev and Fourier model with

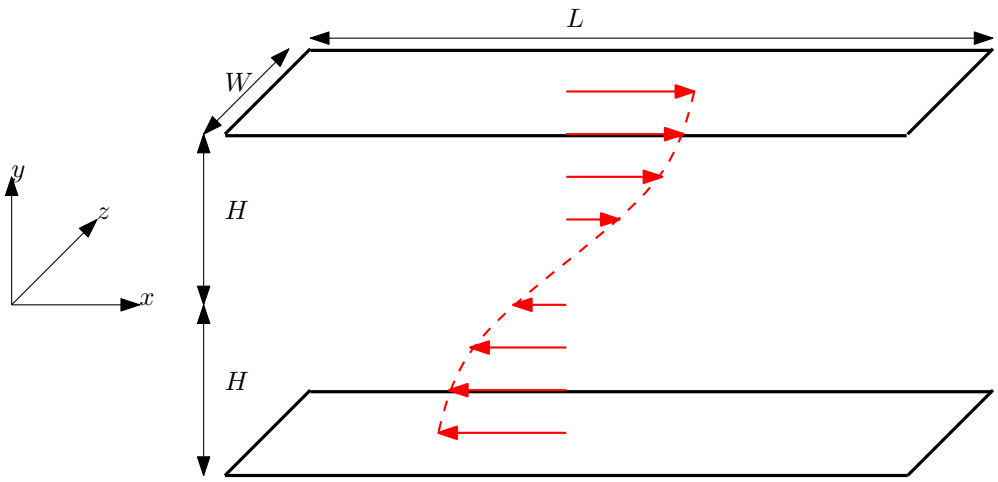

Figure 1.12: The setup for the PCF as modeled by Waleffe

no-slip boundary conditions, but such a model would not be representative of PCF flow. In order to create a relatively accurate low order model of PCF Waleffe changes to the assumptions of PCF:

i) Instead of moving plates we have a body force, $\vec{F} = \overline{U}\left(\sin\left(\frac{\pi y}{2}\right), 0, 0\right)$.

ii) Instead of no-slip we have no-stress boundary conditions at the plates.

The body force is added to compensate for the input of energy by the movement of the infinite plates which we lose by dropping the no-slip boundary conditions. The assumption that the force takes the above form is inspired by the time-averaged flow in PCF [25]. In order to exactly represent the input of energy, Waleffe uses fourier modes in all three directions. Fortunately Fourier modes are eigenfunctions of operators which appear in the NS equation, namely ∂_t, Δ and ∇. This helps in making the model robust even though it is a low-order representation.

The no-slip conditions are replaced with no-stress conditions. The no-stress conditions in the wall-normal direction can be satisfied by some Fourier modes individually. By choosing only those Fourier modes which do satisfy the wall-normal direction the Gibbs phenomenon can be avoided in general. The body force is added to compensate

for the input of energy by the movement of the infinite plates which we lose by dropping the no-slip boundary conditions. The assumption that the force takes the above form is inspired by the time-averaged flow PCF [25].

We now rederive the Waleffe model. First non-dimensionalize the set up with characteristic height $H/2$ and characteristic velocity $\overline{U}$. The transformations are given by:

$$\tilde{x} = \frac{x}{H} \qquad \tilde{y} = \frac{y}{H} \qquad \tilde{z} = \frac{z}{H} \qquad \tilde{\vec{u}} = \frac{1}{\overline{U}}\vec{u} \qquad \tilde{t} = \frac{2\overline{U}}{H}t$$

Henceforth with drop the tilde notation. The domain of interest will be a rectangular prism with periodic boundary conditions on all sides except the surface of the plates. The non-dimensionalized box of interest is then given by:

$$V = \{(x, y, z) \in \mathbb{R}^3 \mid 0 \leq \alpha x, \gamma z < 2\pi, -1 \leq y \leq 1\} \tag{1.5.1}$$

Where $\alpha = \frac{2\pi H}{L}$ and $\gamma = \frac{2\pi H}{W}$ are called the aspect ratios.. The non-dimensionalized force is given by:

$$\vec{F} = (\sin(\pi y/2), 0, 0)$$

The non-dimensionalized Navier-Stokes equations for this setup are:

$$\left(\frac{\partial}{\partial t} - \frac{1}{Re}\nabla^2\right)\vec{u} = -\vec{u}\cdot\nabla\vec{u} - \nabla p + \sin\left(\frac{\pi y}{2}\right)\hat{x} \qquad \nabla\cdot\vec{u} = 0 \tag{1.5.2}$$

with boundary conditions:

$$\begin{aligned} \vec{u}\,(x, y, z) &= \vec{u}\,(x + 2\pi/\alpha, y, z) \\ \vec{u}\,(x, y, z) &= \vec{u}\,(x, y, z + 2\pi/\gamma) \\ v\,(x, \pm 1, z) &= 0 \\ \left.\frac{\partial u}{\partial y}\right|_{y=\pm 1} &= 0 \\ \left.\frac{\partial w}{\partial y}\right|_{y=\pm 1} &= 0 \end{aligned} \tag{1.5.3}$$

Let us consider the symmetries of this system. Define:

$$\begin{aligned} S_z(x,y,z) &= (x,y,-z) \\ S_{xy}(x,y,z) &= (-x,-y,z) \\ T_x(x,y,z) &= (x+\pi/\alpha, y, z) \\ T_z(x,y,z) &= (x,y,z+\pi/\gamma) \end{aligned} \tag{1.5.4}$$

Then, $S_{xy} \circ T_z$ and $S_z \circ T_x$ are symmetries of (1.5.2). That is to say given any solution $\vec{u}$ of (1.5.2), then $S_{xy} \circ T_z(\vec{u})$ and $S_z \circ T_x(\vec{u})$ are also solutions of (1.5.2). This fact becomes important later in our derivation of the low order model. It is important to note that coherent structures as described by the SSP also approximately display these symmetries. .

A solution, $\vec{u}$, of (1.5.2) can be written in terms of its Fourier expansion as follows:

$$\vec{u} = \sum_{\vec{k}\in\mathbb{Z}^3} \vec{a}_{\vec{k}}(t) e^{2\pi i \vec{k}\cdot\vec{x}}$$

Where $\vec{a}_{\vec{k}}(t) \in \mathbb{C}^3 \times \mathbb{R}$. Henceforth we write $\vec{a}_{\vec{k}}$ for $\vec{a}_{\vec{k}}(t)$. We want the solution to be periodic in the streamwise and the spanwise directions. Further we want to allow half wave numbers in the wall-normal direction, so that the sinusoidal force can be represented exactly. For this reason we define:

$$\vec{X} = (\alpha x, \pi y/2, \gamma z)$$

Hence we get an expansion which satisfies the periodic boundary conditions and allows for half wave numbers in wall-normal-direction in the following simplified form:

$$\begin{aligned} \vec{u} &= \sum_{\vec{k}\in\mathbb{Z}^3} \vec{a}_{\vec{k}} e^{i\vec{k}\cdot\vec{X}} \\ &= \sum_{\vec{k}\in\mathbb{Z}^3} \left[a_{1,\vec{k}}\left(e^{i\vec{k}\cdot\vec{X}}\right), a_{2,\vec{k}}\left(e^{i\vec{k}\cdot\vec{X}}\right), a_{3,\vec{k}}\left(e^{i\vec{k}\cdot\vec{X}}\right)\right] \end{aligned}$$

We want to choose basis functions which *individually* satisfy the boundary conditions (1.5.3), the divergence free condition, and the symmetry conditions (1.5.4). The symmetry conditions eliminate traveling wave solutions which would otherwise exist as solutions. However none of the Fourier basis functions can satisfy the boundary

conditions individually. In order to rectify this situation, we will introduce new basis functions.

We know that a solution which represents fluid velocity must be real valued. A sufficient and necessary condition for this is $\vec{a}_{\vec{k}} = \overline{\vec{a}_{\vec{k}}}$. Let us explore what this means. Given $\vec{k} \in \mathbb{Z}^3$ and $a \in \mathbb{C}$, then:

$$\begin{aligned} & ae^{i\left(\vec{k}\cdot\vec{x}\right)} + \overline{a}e^{-i\left(\vec{k}\cdot\vec{x}\right)} \\ &= \Re(a)\left(e^{i\vec{k}\cdot\vec{x}} + e^{-i\vec{k}\cdot\vec{x}}\right) + \Im(a)\left(i\left(e^{i\vec{k}\cdot\vec{x}} - e^{-i\vec{k}\cdot\vec{x}}\right)\right) \end{aligned}$$

Let's expand this further:

$$\begin{aligned} & \Re(a)\left(e^{i\vec{k}\cdot\vec{x}} + e^{-i\vec{k}\cdot\vec{x}}\right) \\ &= \Re(a)\left(e^{i(k_1x+k_2y+k_3z)} + e^{-i(k_1x+k_2y+k_3z)}\right) \\ &= 2\Re(a)\cos\left(k_1x + k_2y + k_3z\right) \\ &= 2\Re(a)\left(\cos\left(k_1x + k_2y\right)\cos\left(k_3z\right) + \sin\left(k_1x + k_2y\right)\sin\left(k_3z\right)\right) \\ &= 2\Re(a)\Big[\left[\cos\left(k_1x\right)\cos\left(k_2y\right) + \sin\left(k_1x\right)\sin\left(k_2y\right)\right]\cos\left(k_3z\right) \\ &\qquad + \left[\sin\left(k_1x\right)\cos\left(k_2y\right) + \cos\left(k_1x\right)\sin\left(k_2y\right)\right]\sin\left(k_3z\right)\Big] \\ &= 2\Re(a)\Big[\cos\left(k_1x\right)\cos\left(k_2y\right)\cos\left(k_3z\right) + \sin\left(k_1x\right)\sin\left(k_2y\right)\cos\left(k_3z\right) \\ &\qquad + \sin\left(k_1x\right)\cos\left(k_2y\right)\sin\left(k_3z\right) + \cos\left(k_1x\right)\sin\left(k_2y\right)\sin\left(k_3z\right)\Big] \end{aligned}$$

Similarly we find:

$$\begin{aligned} & \Im(a)\left(i\left(e^{i\vec{k}\cdot\vec{x}} - e^{-i\vec{k}\cdot\vec{x}}\right)\right) \\ = \; & -2\Im(a)\Big[\cos\left(k_1x\right)\cos\left(k_2y\right)\sin\left(k_3z\right) + \cos\left(k_1x\right)\sin\left(k_2y\right)\cos\left(k_3z\right) \\ &\qquad + \sin\left(k_1x\right)\cos\left(k_2y\right)\cos\left(k_3z\right) + \sin\left(k_1x\right)\sin\left(k_2y\right)\sin\left(k_3z\right)\Big] \end{aligned}$$

From this we can easily see that we have the following identities:

$$
\begin{aligned}
& ae^{i(k_1x+k_2y+k_3z)} + \overline{a}e^{-i(k_1x+k_2y+k_3z)} \\
= \; & 2\Re(a)\Big[\cos(k_1x)\cos(k_2y)\cos(k_3z) + \sin(k_1x)\sin(k_2y)\cos(k_3z) \\
& \quad + \sin(k_1x)\cos(k_2y)\sin(k_3z) + \cos(k_1x)\sin(k_2y)\sin(k_3z)\Big] \\
& -2\Im(a)\Big[\cos(k_1x)\cos(k_2y)\sin(k_3z) + \cos(k_1x)\sin(k_2y)\cos(k_3z) \\
& \quad + \sin(k_1x)\cos(k_2y)\cos(k_3z) + \sin(k_1x)\sin(k_2y)\sin(k_3z)\Big]
\end{aligned}
$$

$$
\begin{aligned}
& ae^{i(-k_1x+k_2y+k_3z)} + \overline{a}e^{-i(-k_1x+k_2y+k_3z)} \\
= \; & 2\Re(a)\Big[\cos(k_1x)\cos(k_2y)\cos(k_3z) - \sin(k_1x)\sin(k_2y)\cos(k_3z) \\
& \quad - \sin(k_1x)\cos(k_2y)\sin(k_3z) + \cos(k_1x)\sin(k_2y)\sin(k_3z)\Big] \\
& -2\Im(a)\Big[\cos(k_1x)\cos(k_2y)\sin(k_3z) + \cos(k_1x)\sin(k_2y)\cos(k_3z) \\
& \quad - \sin(k_1x)\cos(k_2y)\cos(k_3z) + \sin(k_1x)\sin(k_2y)\sin(k_3z)\Big]
\end{aligned}
$$

$$
\begin{aligned}
& ae^{i(k_1x-k_2y+k_3z)} + \overline{a}e^{-i(k_1x-k_2y+k_3z)} \\
= \; & 2\Re(a)\Big[\cos(k_1x)\cos(k_2y)\cos(k_3z) - \sin(k_1x)\sin(k_2y)\cos(k_3z) \\
& \quad + \sin(k_1x)\cos(k_2y)\sin(k_3z) - \cos(k_1x)\sin(k_2y)\sin(k_3z)\Big] \\
& -2\Im(a)\Big[\cos(k_1x)\cos(k_2y)\sin(k_3z) - \cos(k_1x)\sin(k_2y)\cos(k_3z) \\
& \quad + \sin(k_1x)\cos(k_2y)\cos(k_3z) - \sin(k_1x)\sin(k_2y)\sin(k_3z)\Big]
\end{aligned}
$$

$$
\begin{aligned}
& ae^{i(k_1x+k_2y-k_3z)} + \overline{a}e^{-i(k_1x+k_2y-k_3z)} \\
= \; & 2\Re(a)\Big[\cos(k_1x)\cos(k_2y)\cos(k_3z) + \sin(k_1x)\sin(k_2y)\cos(k_3z) \\
& \quad - \sin(k_1x)\cos(k_2y)\sin(k_3z) - \cos(k_1x)\sin(k_2y)\sin(k_3z)\Big] \\
& -2\Im(a)\Big[-\cos(k_1x)\cos(k_2y)\sin(k_3z) + \cos(k_1x)\sin(k_2y)\cos(k_3z) \\
& \quad + \sin(k_1x)\cos(k_2y)\cos(k_3z) - \sin(k_1x)\sin(k_2y)\sin(k_3z)\Big]
\end{aligned}
$$

This shows that the basis $\mathfrak{B}_1$ and $\mathfrak{B}_2$ defined below are equivalent:

$$\begin{aligned}\mathfrak{B}_1 = \Big\{ & e^{i(+k_1x+k_2y+k_3z)} + e^{-i(+k_1x+k_2y+k_3z)}, \\ & e^{i(+k_1x+k_2y+k_3z)} - e^{-i(+k_1x+k_2y+k_3z)}, \\ & e^{i(-k_1x+k_2y+k_3z)} + e^{-i(-k_1x+k_2y+k_3z)}, \\ & e^{i(-k_1x+k_2y+k_3z)} - e^{-i(-k_1x+k_2y+k_3z)}, \\ & e^{i(+k_1x-k_2y+k_3z)} + e^{-i(+k_1x-k_2y+k_3z)}, \\ & e^{i(+k_1x-k_2y+k_3z)} - e^{-i(+k_1x-k_2y+k_3z)}, \\ & e^{i(+k_1x+k_2y-k_3z)} + e^{-i(+k_1x+k_2y-k_3z)}, \\ & e^{i(+k_1x+k_2y-k_3z)} - e^{-i(+k_1x+k_2y-k_3z)} \Big\}\end{aligned}$$

$$\begin{aligned}\mathfrak{B}_2 = \Big\{ & \sin(k_1x)\sin(k_2y)\sin(k_3z), \\ & \sin(k_1x)\sin(k_2y)\cos(k_3z), \\ & \sin(k_1x)\cos(k_2y)\sin(k_3z), \\ & \cos(k_1x)\sin(k_2y)\sin(k_3z), \\ & \sin(k_1x)\cos(k_2y)\cos(k_3z), \\ & \cos(k_1x)\sin(k_2y)\cos(k_3z), \\ & \cos(k_1x)\cos(k_2y)\sin(k_3z), \\ & \cos(k_1x)\cos(k_2y)\cos(k_3z) \Big\}\end{aligned}$$

Both of these are a basis for the space of real-valued functioned that can be written as a linear combination of Fourier basis functions with wave numbers (l_1, l_2, l_3) such that $\|l_1\| = k_1$, $\|l_2\| = k_2$ and $\|l_3\| = k_3$.

We now return to the original problem of representing the velocity field of a fluid using basis functions which individually satisfy the divergence free condition, the boundary conditions, and the symmetries. The functions in $\mathbb{B}_2$ can be used to create such a

basis. We write a 3-vector using elements of $\mathbb{B}_2$ in the form:

$$\begin{aligned}\vec{\nu} &= [\nu_1, \nu_2, \nu_3] \\ &= \Big[c_1 \left(e^{i\alpha k_1 x} \pm e^{-i\alpha k_1 x}\right) \left(e^{i\pi k_2 y/2} \pm e^{-i\pi k_2 y/2}\right) \left(e^{i\gamma k_2 z} \pm e^{-i\gamma k_3 z}\right), \\ &\quad c_2 \left(e^{i\alpha k_1 x} \pm e^{-i\alpha k_1 x}\right) \left(e^{i\pi k_2 y/2} \pm e^{-i\pi k_2 y/2}\right) \left(e^{i\gamma k_2 z} \pm e^{-i\gamma k_3 z}\right), \\ &\quad c_3 \left(e^{i\alpha k_1 x} \pm e^{-i\alpha k_1 x}\right) \left(e^{i\pi k_2 y/2} \pm e^{-i\pi k_2 y/2}\right) \left(e^{i\gamma k_3 z} \pm e^{-i\gamma k_3 z}\right) \Big]\end{aligned}$$

Where each $\pm$ can be chosen independently and $c_i \in \{1, 0, i\}$. The choice of c_i must be such that each component must be real valued. Some of these functions will individually satisfy the boundary conditions (1.5.3), the divergence free condition, and the symmetry conditions (1.5.4). Call this set $\Gamma_{\vec{k}}$. One problem is that the set $\Gamma_{\vec{k}}$ is not linearly independent. We will have to sieve the functions to find those which satisfy the above mentioned properties and then choose a linearly independent subset of them.

First consider the divergence free condition. We want $\vec{\nu} \in \Gamma_{\vec{k}}$ to satisfy $\nabla \cdot \vec{\nu} = 0$. This can be written as:

$$\begin{aligned}\nabla \cdot \vec{\nu} &= \frac{\partial \nu_1}{\partial x} + \frac{\partial \nu_1}{\partial y} + \frac{\partial \nu_1}{\partial z} \\ &= \quad \alpha k_1 c_1 \left(e^{i\alpha k_1 x} \mp e^{-i\alpha k_1 x}\right) \left(e^{i\pi k_2 y/2} \pm e^{-i\pi k_2 y/2}\right) \left(e^{i\gamma k_2 z} \pm e^{-i\gamma k_3 z}\right) \\ &\quad + \frac{1}{2} k_2 c_2 \left(e^{i\alpha k_1 x} \pm e^{-i\alpha k_1 x}\right) \left(e^{i\pi k_2 y/2} \mp e^{-i\pi k_2 y/2}\right) \left(e^{i\gamma k_2 z} \pm e^{-i\gamma k_3 z}\right) \\ &\quad + \gamma k_3 c_3 \left(e^{i\alpha k_1 x} \pm e^{-i\alpha k_1 x}\right) \left(e^{i\pi k_2 y/2} \pm e^{-i\pi k_2 y/2}\right) \left(e^{i\gamma k_3 z} \mp e^{-i\gamma k_3 z}\right) \\ &= 0\end{aligned}$$

From this it can be readily seen that the $\pm$ can not be chosen independently of each other. In fact the $\pm$ and $\mp$ where vertically aligned must be dependent. Then our spanning set is given by functions of the form:

$$\begin{aligned}\vec{\nu} &= [\nu_1, \nu_2, \nu_3] \\ &= \Big[c_1 \left(e^{i\alpha k_1 x} \pm_1 e^{-i\alpha k_1 x}\right) \left(e^{i\pi k_2 y/2} \mp_2 e^{-i\pi k_2 y/2}\right) \left(e^{i\gamma k_2 z} \mp_3 e^{-i\gamma k_3 z}\right), \\ &\quad c_2 \left(e^{i\alpha k_1 x} \mp_1 e^{-i\alpha k_1 x}\right) \left(e^{i\pi k_2 y/2} \pm_2 e^{-i\pi k_2 y/2}\right) \left(e^{i\gamma k_2 z} \mp_3 e^{-i\gamma k_3 z}\right),\end{aligned}$$

$$c_3 \left(e^{i\alpha k_1 x} \mp_1 e^{-i\alpha k_1 x}\right) \left(e^{i\pi k_2 y/2} \mp_2 e^{-i\pi k_2 y/2}\right) \left(e^{i\gamma k_3 z} \pm_3 e^{-i\gamma k_3 z}\right) \Bigg]$$

Where the dependence of the signs has been made clear by the index notation. Call this new set of functions $\Gamma'_{\vec{k}}$. We can now write an algorithm to isolate for any $\vec{k}$ a linearly independent of subset $\Gamma'_{\vec{k}}$, all of whose elements satisfy:

1. The divergence free condition
$$c_1 \alpha k_1 + \frac{1}{2} c_2 k_2 + c_3 \gamma k_3 = 0 \tag{1.5.5}$$
2. The stress-free conditions and the zero wall-normal velocity condition become:
$$\begin{aligned} c_1 k_2/2 \left(e^{i\pi k_2/2} \mp e^{-i\pi k_2/2}\right) &= 0 \\ c_2 \left(e^{i\pi k_2/2} \pm e^{-i\pi k_2/2}\right) &= 0 \\ c_3 k_2/2 \left(e^{i\pi k_2/2} \mp e^{-i\pi k_2/2}\right) &= 0 \end{aligned}$$
3. The symmetry conditions (1.5.4).

If we allow wave numbers $[-1, 0, 1]$ in each direction then we get the following linearly independent set of functions with the desired properties. Some of these basis functions represent coherent structures while others represent instability modes. These are the basis functions used by Waleffe [25] in his model of shear of flow:

$$\begin{aligned} \phi_1 &= \left[\frac{1}{2} \frac{\sin\left(\frac{1}{2}\pi y\right)}{\pi \sqrt{\frac{1}{\gamma\alpha}}},\ 0\ ,\ 0\right] \\ \phi_2 &= \left[\frac{1}{2} \frac{\cos\left(\gamma z\right)}{\pi \sqrt{\frac{1}{\gamma\alpha}}},\ 0\ ,\ 0\right] \\ \phi_3 &= \left[0\ ,\ \frac{\sqrt{2}\gamma \cos\left(\frac{1}{2}\pi y\right) \cos\left(\gamma z\right)}{\pi \sqrt{\frac{4\gamma^2+\pi^2}{\gamma\alpha}}},\ \frac{1}{2} \frac{\sqrt{2} \sin\left(\frac{1}{2}\pi y\right) \sin\left(\gamma z\right)}{\pi \sqrt{\frac{4\gamma^2+\pi^2}{\gamma\alpha}}}\right] \end{aligned}$$

$$\phi_4 = \left[0\ ,\ 0\ , \frac{1}{2}\frac{\cos(\alpha x)}{\pi\sqrt{\frac{1}{\gamma\alpha}}}\right]$$

$$\phi_5 = \left[-\frac{1}{2}\frac{\sqrt{2}\gamma\cos(\alpha x)\sin(\gamma z)}{\pi\sqrt{\frac{\alpha^2+\gamma^2}{\gamma\alpha}}},\ 0\ , \frac{1}{2}\frac{\sqrt{2}\alpha\sin(\alpha x)\cos(\gamma z)}{\pi\sqrt{\frac{\alpha^2+\gamma^2}{\gamma\alpha}}}\right]$$

$$\phi_6 = \left[0\ ,\ 0\ , \frac{1}{2}\frac{\sqrt{2}\sin(\alpha x)\sin\left(\frac{1}{2}\pi y\right)}{\pi\sqrt{\frac{1}{\gamma\alpha}}}\right]$$

$$\phi_7 = \left[\frac{\gamma\sin(\alpha x)\sin\left(\frac{1}{2}\pi y\right)\sin(\gamma z)}{\pi\sqrt{\frac{\alpha^2+\gamma^2}{\gamma\alpha}}},\ 0\ , \frac{\alpha\cos(\alpha x)\sin\left(\frac{1}{2}\pi y\right)cos(\gamma z)}{\pi\sqrt{\frac{\alpha^2+\gamma^2}{\gamma\alpha}}}\right]$$

$$\phi_8 = \left[\frac{\alpha\sin(\alpha x)\sin\left(\frac{1}{2}\pi y\right)\sin(\gamma z)}{\sqrt{\frac{(\alpha^2+\gamma^2)(4\alpha^2+\pi^2+4\gamma^2)}{\gamma\alpha}}}, \frac{2(\alpha^2+\gamma^2)\cos(\alpha x)\cos\left(\frac{1}{2}\pi y\right)\sin(\gamma z)}{\pi\sqrt{\frac{(\alpha^2+\gamma^2)(4\alpha^2+\pi^2+4\gamma^2)}{\gamma\alpha}}},\right.$$
$$\left.\frac{-\gamma\cos(\alpha x)\sin\left(\frac{1}{2}\pi y\right)\cos(\gamma z)}{\sqrt{\frac{(\alpha^2+\gamma^2)(4\alpha^2+\pi^2+4\gamma^2)}{\gamma\alpha}}}\right]$$

Here ϕ_1 is the main shear mode, ϕ_2 is a streak mode, ϕ_3 is a roll mode, and the rest are instability modes. Note that by we inherit from the construction the following inner product:

$$\begin{aligned}\langle\phi_i,\phi_j\rangle &= \int_V (\phi_i\cdot\phi_j)\ dV \\ &= \int_0^{2\pi/\gamma}\int_{-1}^{1}\int_0^{2\pi/\alpha} (\phi_i\cdot\phi_j)\ dxdydz \\ &= \delta_{ij}\end{aligned} \tag{1.5.6}$$

Where V is the box specified in (1.5.1). We can now give the following approximate expansion of a solution $\vec{u}$ of (1.5.2).

$$\vec{u} \approx \sum_{i=1}^{8} a_i\ \phi_i$$

Plugging the above into (1.5.2) we get:

$$\begin{aligned}&\frac{\partial}{\partial t}\sum_{i=1}^{8} a_i\phi_i\\ =&\frac{1}{Re}\nabla^2\left(\sum_{i=1}^{8} a_i\phi_i\right)-\left(\sum_{i=1}^{8} a_i\phi_i\cdot\nabla\right)\sum_{i=1}^{8} a_i\phi_i-\nabla p+\phi_1\end{aligned}$$

Now consider the projection of the above equation on a fixed basis function ϕ_k:

$$\begin{aligned}&\left\langle\frac{\partial}{\partial t}\sum_{i=1}^{8} a_i\phi_i,\phi_k\right\rangle\\ =&\left\langle\frac{1}{Re}\nabla^2\left(\sum_{i=1}^{8} a_i\phi_i\right)-\left(\sum_{i=1}^{8} a_i\phi_i\cdot\nabla\right)\sum_{i=1}^{8} a_i\phi_i-\nabla p+\phi_1,\phi_k\right\rangle\end{aligned}\tag{1.5.7}$$

Let's consider each component of (1.5.7) individually. First we have:

$$\begin{aligned}\left\langle\frac{\partial}{\partial t}\sum_{i=1}^{8} a_i\phi_i,\phi_k\right\rangle&=\sum_{i=1}^{8}\frac{\partial a_i}{\partial t}\left\langle\phi_i,\phi_k\right\rangle\\ &=\sum_{i=1}^{8}\dot{a_i}\delta_{ik}\\ &=\dot{a_k}\end{aligned}$$

Next we have:

$$\begin{aligned}\left\langle\frac{1}{Re}\nabla^2\left(\sum_{i=1}^{8} a_i\phi_i\right),\phi_k\right\rangle&=\frac{1}{Re}\sum_{i=1}^{8} a_iL_i\left\langle\phi_i,\phi_k\right\rangle\\ &=\frac{L_k}{Re}a_k\end{aligned}$$

Where $\nabla^2\phi_i=L_i\phi_i$, since ϕ_i are eigenvectors of ∇^2. Next, we have the non-linear terms:

$$\begin{aligned}\left\langle\left(\sum_{i=1}^{8} a_i\phi_i\cdot\nabla\right)\sum_{i=1}^{8} a_i\phi_i,\phi_k\right\rangle&=\left\langle\left(\sum_{i=1}^{8} a_i\phi_i\cdot\nabla\right)\sum_{j=1}^{8} a_j\phi_j,\phi_k\right\rangle\\ &=\left\langle\sum_{i=1}^{8}\sum_{j=1}^{8} a_ia_j\left(\phi_i\cdot\nabla\phi_j\right),\phi_k\right\rangle\end{aligned}$$

$$= \sum_{i=1}^{8} \sum_{j=1}^{8} a_i a_j \left\langle \left(\phi_i \cdot \nabla \phi_j \right), \phi_k \right\rangle$$
$$= a^T S_k a$$

Where a is the vector $(a_1, ..., a_8)$ and S_k is the matrix with elements given by:

$$[S_k]_{i,j} = \left\langle \left(\phi_i \cdot \nabla \phi_j \right), \phi_k \right\rangle$$

The projection of the non-linear terms has to be calculated individually for each ϕ_k using (1.5.6). Next consider the pressure:

$$\begin{aligned}
\langle \nabla p, \phi_k \rangle &= \int_V \left(\nabla p \cdot \phi_k \right) \, dV \\
&= \int_V \left(\nabla \cdot \left(p \phi_k \right) - p \left(\nabla \cdot \phi_k \right) \right) \, dV \\
&= \int_V \left(\nabla \cdot \left(p \phi_k \right) \right) \, dV \\
&= \int_{\partial S} p \phi_k \cdot \vec{n} \, dS \\
&= 0
\end{aligned}$$

Where we have used standard identities to simplify the equation. The last equality follows from the fact that ϕ_k is periodic in four direction and zero in the wall normal direction at the plates. Finally for the body force we have:

$$\begin{aligned}
\left\langle \vec{F}, \phi_k \right\rangle &= \langle \phi_1, \phi_k \rangle \\
&= \delta_{1k} \phi_k
\end{aligned}$$

Thus we get a system of ODEs, satisfying:

$$\frac{da_k}{dt} = \frac{L_k}{Re} a_k + a^T S_k a + \delta_{1k} \phi_k \tag{1.5.8}$$

Where L_k are real-valued coefficients and S_k are 8×8 matrices with real-valued coefficients.

In his seminal paper, Waleffe showed that this simple system of ODE's captures many properties of PCF. For example the mean velocity profile is approximately the same as the mean velocity profile for PCF. Another similarity is that we are able to find a non-trivial solution which is analogous to the one found by Nagata. Finally and most importantly this simple model displays the SSP process very clearly.

We extend the model of Waleffe to include wave number $[-3,-2,-1,0,1,2,3]$ in the wall normal direction. The following are the additional basis functions which are added to the system:

$$\phi_9 = \left[\frac{1}{2}\frac{\sqrt{2}\cos(\pi y)\cos(\gamma z)}{\pi\sqrt{\frac{1}{\gamma\alpha}}},\ 0\ ,\ 0\right]$$

$$\phi_{10} = \left[0\ ,\ 0\ ,\frac{1}{2}\frac{\sqrt{2}\cos(\alpha x)\cos(\pi y)}{\pi\sqrt{\frac{1}{\gamma\alpha}}}\right]$$

$$\phi_{11} = \left[-\frac{\gamma\cos(\alpha x)\cos(\pi y)\sin(\gamma z)}{\pi\sqrt{\frac{\alpha^2+\gamma^2}{\gamma\alpha}}},\ 0\ ,\frac{\alpha\sin(\alpha x)\cos(\pi y)\cos(\gamma z)}{\pi\sqrt{\frac{\alpha^2+\gamma^2}{\gamma\alpha}}}\right]$$

$$\phi_{12} = \left[\frac{\alpha\cos(\alpha x)\cos(\pi y)\sin(\gamma z)}{\sqrt{\frac{(\alpha^2+\gamma^2)(\alpha^2+\pi^2+\gamma^2)}{\gamma\alpha}}},\frac{(\alpha^2+\gamma^2)\sin(\alpha x)\sin(\pi y)\sin(\gamma z)}{\pi\sqrt{\frac{(\alpha^2+\gamma^2)(\alpha^2+\pi^2+\gamma^2)}{\gamma\alpha}}},\right.$$
$$\left.\frac{-\gamma\sin(\alpha x)\cos(\pi y)\cos(\gamma z)}{\sqrt{\frac{(\alpha^2+\gamma^2)(\alpha^2+\pi^2+\gamma^2)}{\gamma\alpha}}}\right]$$

$$\phi_{13} = \left[\frac{1}{2}\frac{\sin\left(\frac{3}{2}\pi y\right)}{\pi\sqrt{\frac{1}{\gamma\alpha}}},\ 0\ ,\ 0\right]$$

$$\phi_{14} = \left[0\ ,\ \frac{\sqrt{2}\gamma\cos\left(\frac{3}{2}\pi y\right)\cos(\gamma z)}{\pi\sqrt{\frac{4\gamma^2+9\pi^2}{\gamma\alpha}}},\ \frac{3}{2}\frac{\sqrt{2}\sin\left(\frac{3}{2}\pi y\right)\sin(\gamma z)}{\pi\sqrt{\frac{4\gamma^2+9\pi^2}{\gamma\alpha}}}\right]$$

$$\phi_{15} = \left[0\ ,\ 0\ ,\frac{1}{2}\frac{\sqrt{2}\sin(\alpha x)\sin\left(\frac{3}{2}\pi y\right)}{\pi\sqrt{\frac{1}{\gamma\alpha}}}\right]$$

$$\phi_{16} = \left[\frac{\alpha\sin(\alpha x)\sin\left(\frac{3}{2}\pi y\right)\sin(\gamma z)}{\pi\sqrt{\frac{\alpha^2+\gamma^2}{\gamma\alpha}}},\ 0\ ,\frac{\alpha\cos(\alpha x)\sin\left(\frac{3}{2}\pi y\right)cos(\gamma z)}{\pi\sqrt{\frac{\alpha^2+\gamma^2}{\gamma\alpha}}}\right]$$

$$\phi_{17} = \left[\frac{3\alpha \sin(\alpha x) \sin\left(\frac{3}{2}\pi y\right) \sin(\gamma z)}{\sqrt{\frac{(\alpha^2+\gamma^2)(4\alpha^2+9\pi^2+4\gamma^2)}{\gamma\alpha}}}, \frac{2(\alpha^2+\gamma^2)\cos(\alpha x)\cos\left(\frac{3}{2}\pi y\right)\sin(\gamma z)}{\pi\sqrt{\frac{(\alpha^2+\gamma^2)(4\alpha^2+9\pi^2+4\gamma^2)}{\gamma\alpha}}}, \right.$$
$$\left. \frac{-3\gamma \cos(\alpha x) \sin\left(\frac{3}{2}\pi y\right) \cos(\gamma z)}{\sqrt{\frac{(\alpha^2+\gamma^2)(4\alpha^2+9\pi^2+4\gamma^2)}{\gamma\alpha}}} \right]$$

Where ϕ_9 is a shear mode, ϕ_{13} is a streak mode, ϕ_{14} is a roll mode, and the rest are instability modes. We now construct a system of ODEs like (1.5.8), but using all 17 modes:

$$\frac{da_k}{dt} = \frac{L_k}{Re} a_k + a^T S_k a + \delta_{1k}\phi_k \qquad , \qquad 1 \leq k \leq 17 \tag{1.5.9}$$

Where S_k and L_k and are modified accordingly. Henceforth we refer to (1.5.9) as the Extended Waleffe Model (EWM). This extended model was first used in [20] and then later in [21]. The benefit of this extended model is in the results of the bifurcation analysis of it. In the next chapter we introduce the theory of bifurcation analysis and explore the implications of it for this model.

Dynamical Systems Analysis and Applications

The study of physical phenomenon has given rise to many differential equations which model them. These differential equations in many cases describe the physical phenomenon with a very high degree of accuracy. The aim of studying these models is to better understand the physical phenomenon itself . However it is cumbersome to study many specific solutions of a model to gain insight into the model as a whole. Consider for example our discussion on Rayleigh-Bénard convection in Section 1.4.5. We could have numerically simulated solutions near the equilibrium point for varying values of the parameter R (Rayleigh number). However instead of doing that we analytically studied the linear stability of the equilibrium solution as it depends on R. In this way we can describe the behavior around the equilibrium qualitatively. For example in the case of Rayleigh-Bénard convection we found that at a certain value of R the behavior of the system changes qualitatively; this is called a bifurcation. The study of the qualitative behavior near a solution of a dynamical system is called bifurcation Theory.

The above example from Rayleigh-Bénard convection is an example of studying the qualitative behavior around an equilibrium solution. We can also study the qualitative behavior around periodic solutions using bifurcation theory. Recall from Section 1.5.1 that there are periodic solutions to PCF and that we are interested in connecting orbits between periodic solutions. These orbits would help us to better understand turbulence. We can find an analogous periodic solutions for the EWM. We are now interested in studying the qualitative behavior around this periodic solution to better understand turbulence.

Finding bifurcations using analytic methods as we did in the Rayleigh-Bénard case is generally not possible. Luckily we can study bifurcations numerically using the method of parameter continuation. Parameter continuation is a numerical method to find a parametrized curve of solutions for an under-determined system of equations. Using this method we can find bifurcations of a dynamical system that occur along that curve of solutions. An example of a parameter continuation software is MatCont which is written in Matlab [5]. There are many types of bifurcations both for equilibrium solutions and periodic solutions. Each bifurcation has an associated co-dimension, which will be introduced in Section 2.1 . Bifurcation are classified based on their co-dimension. The dynamics near a bifurcation of co-dimension 1 and co-dimension 2 for an equilibrium solution has been extensively studied and are well understood. Co-dimension 1 bifurcations for periodic solutions have also been extensively studied. However the classification of co-dimension 2 bifurcations of periodic solutions is much more recent. One type of co-dimension 2 bifurcation for periodic solutions is the LPNS (Limit-Point Neimark-Sacker) bifurcation. Using parameter continuation methods van Veen found a bifurcation of type LPNS for the periodic solution associated with the EWM [20]. The description of the dynamics near this bifurcation was provided through two examples by Vitolo [23]. Bifurcation theory tells us, under certain conditions, that there are connected orbits between periodic orbits near this type of bifurcation.

A very useful tool in the study of dynamical systems is normal forms. We can rewrite a dynamical system in a somewhat standard form for each type of bifurcation. We can also analytically study the dynamics near each type of dynamical system using the normal form. Then when we detect a bifurcation through numerical methods we can use the information we have about the normal form of that type of bifurcation to predict the behavior. The normal form for the LPNS bifurcation was first derived as part of Virginie De Witte's PhD dissertation [4], along with numerical computations of LPNS points in MatCont. One of the aims of this thesis is to explore the dynamics of that periodic solution near the LPNS bifurcation found by van Veen.

In this chapter we will introduce the standard definitions and methods used in bifurcation Theory and parameter continuation. After introducing the basic definitions and preliminary results we will describe the dynamics around the LPNS bifurcation. We will follow the thesis of De Witte [4] closely in doing it. We will also use notions from [27] for the theory of dynamical systems. We will then introduce MatCont and present the results of parameter continuation on the periodic solution.

2.1 Dynamical Systems

Consider the EWM given by (1.5.9). We can write the system in the form:

$$\begin{aligned}
\frac{da_1}{dt} &= \frac{L_1}{Re}a_1 + a^T S_1 a + \phi_1 \\
\frac{da_2}{dt} &= \frac{L_2}{Re}a_2 + a^T S_2 a \\
&\vdots \\
\frac{da_{17}}{dt} &= \frac{L_{17}}{Re}a_{17} + a^T S_{17} a
\end{aligned}$$

Or alternatively we can write:

$$\dot{a} = f\left(a, Re\right)$$

Here the vector of co-ordinates $a = (a_1, ..., a_{17})$ is called the state vector. The Reynolds number, Re, is a parameter on which the system depends. We have assumed that the coordinates of a depend continuously on time, $t \in \mathbb{R}$. This system only depends on time implicitly (through the vector a). It does not depend on time explicitly, as such it is called an autonomous system. Generically an autonomous system of differential equations can depend on more than one parameter and then we write $\vec{\alpha}$ for vector whose co-ordinates are given by the parameters.

Generically a continuous-time autonomous dynamical system can be written as:

$$\dot{x} = f\left(x, \alpha\right) \tag{2.1.1}$$

Where $x \in \mathbb{R}^n$ are the coordinates in that state-space and $\alpha \in \mathbb{R}^p$ the coordinates in the parameter space. We write $f : \mathbb{R}^n \times \mathbb{R}^p \to \mathbb{R}^n$. We wish to talk about solutions of dynamical systems and we now formalize that concept.

Definition 2.1. *Given an interval of time $I \in \mathbb{R}$, then a **solution of** (2.1.1) is a function $X : I \to \mathbb{R}^n$ which takes t to $X(t)$ and satisfies: $\dot{X}(t) = f(X(t), \alpha)$*

The existence of solutions to (2.1.1) depends on the degree of differentiability of f. In general for any point $x_0 \in \mathbb{R}^n$, time $t_0 \in \mathbb{R}$, and parameters $\alpha_0 \in \mathbb{R}^p$, there exists a unique solution with the same degree of smoothness as f for some finite time interval I with $t_0 \in I$. In our model (1.5.8), $f \in C^\infty$ i.e f is infinitely differentiable, hence we are guaranteed the existence and sufficient smoothness of solutions. We now formalize the concept of a dynamical system.

Definition 2.2. *An **evolution operator** is a map $\phi^t : \mathbb{R}^n \to \mathbb{R}^n$, from the state space $\mathbb{R}^n$ to itself. A family of such maps $\{\phi^t\}_{t\in I}$ for some time interval I is called the **flow**. Suppose $0 \in I$, then a **dynamical system** associated with (2.1.1) is a triplet $\{I, \mathbb{R}^n, \{\phi^t\}_{t\in I}\}$ such that:*

1. $\phi^0 = id$
2. $\phi^t \cdot \phi^s = \phi^{t+s}$
3. $\dot{\phi}^t(x) = f(\phi^t(x), \alpha), \ \forall x \in \mathbb{R}^n$

Henceforth we write ϕ^t for the flow instead of $\{\phi^t\}_{t\in I}$, but it is assumed that the family is parametrized by t in a given time interval. We know that for any point in the state-space with fixed parameters there is a unique solution of (2.1.1) in a neighborhood of that point. In this way we can associate a dynamical system with solutions of (2.1.1). We use the above definition of a dynamical system in defining bifurcations through the concept of topological equivalence as will be seen in Definition 2.9. We can now define some basic intuitive notions about a dynamical system. Given a dynamical system $\{I, \mathbb{R}^n, \phi^t\}_{t\in I}$ and a point $x_0 \in \mathbb{R}^n$ we have:

Definition 2.3. *. If x_0 satisfies $\phi^t(x_0) = x_0$ for all $t \in I$ then it is an **equilibrium** point.*

Definition 2.4. *If there exists a minimal $T_0 > 0$ such that $\phi^{T_0}(x_0) = x_0$, then the set $\{\ \phi^t(x_0)\ \mid 0 \le t < T_0\ \}$ is called a **periodic orbit** with **period** T_0.*

Definition 2.5. *A periodic orbit is called a **limit cycle** if there are no other periodic orbits in some neighborhood of it. .*

Definition 2.6. *Let O_1 and O_2 be a periodic orbits. Suppose there exist x_0 such that:*

$$\lim_{t\to-\infty} \phi^t(x_0) \in O_1 \quad \text{and} \quad \lim_{t\to+\infty} \phi^t(x_0) \in O_1$$

*Then the set $\{\ \phi^t(x_0)\ \mid t \in \mathbb{R}\ \}$ is called a **heteroclinic orbit** if O_1 and O_2 are different and a **homoclinic orbit** if they are the same.*

Definition 2.7. *A set $S \subset \mathbb{R}^n$ with the property that $\phi^t(s) \in S$ for all $s \in S$ and $t \in I$ is an **invariant set**.*

We then observe that fixed points, periodic orbits, homoclinic orbits and heteroclinic orbits are all examples of invariant sets according to the above definition. Next we want to define an equivalence relation on dynamical systems.

Definition 2.8. *Two dynamical systems, $\{I, \mathbb{R}^n, \phi^t\}$ and $\{I, \mathbb{R}^n, \psi^t\}$ are **topologically equivalent** if there is a homeomorphism $h : \mathbb{R}^n \to \mathbb{R}^n$ such that for all $x \in \mathbb{R}^n$ we have:*

$$\{h(\psi(x,t)) \,|t \in I\} = \{\phi(h(x),t) \,|t \in I\}$$

and additionally the direction of time is also preserved.

While this definition seems cumbersome it is essentially what one imagines it means for two phase portraits to be topologically equivalent. For example consider the system:

$$\begin{aligned} \dot{x} &= \alpha - x^2 \\ \dot{y} &= -y \end{aligned} \tag{2.1.2}$$

If $\alpha < 0$ then this system doesn't have any equilibrium solutions, if $\alpha = 0$ then there is one equilibrium solution at $(0,0)$, finally if $\alpha > 0$ then there are two equilibrium at $(\pm\sqrt{\alpha}, 0)$. The dynamics around these points upto topological equivalence is shown in Figure 2.1.

We are now ready to to formalize the concept of bifurcation using the notion of topological equivalence.

Definition 2.9. *A **bifurcation** is a point in parameter space whose every neighborhood contains at least two topologically inequivalent dynamical systems.*

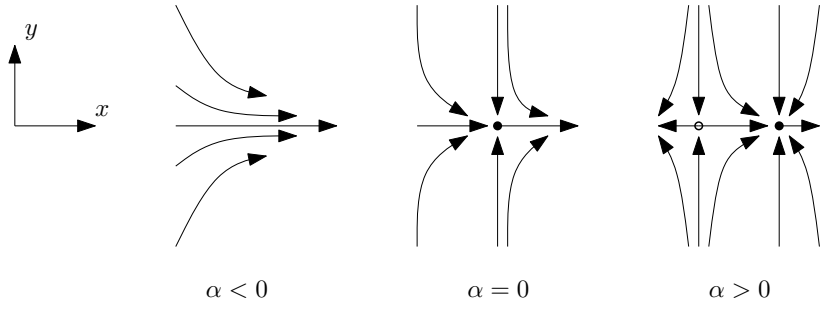

Figure 2.1: Phase portraits for (2.1.2)

Bifurcation points can be classified based on the topologically inequivalent phase portraits around them. For any given bifurcation point, we can associate a **bifurcation set**, which is a connected component of the parameter space whose every point is a bifurcation point of the same type.

Definition 2.10. *For a finite-dimensional parameter space, the **co-dimension** of a bifurcation set is the difference between the dimension of the parameter space and that of the bifurcation set.*

A bifurcation diagram is often used to separate (in parameter space) regions in which all dynamical systems are topologically invariant to each other. An example of a bifurcation diagram for (2.1.2) is shown below in Figure 2.4

Definition 2.11. *The **Jacobian** of $f(x, \alpha)$ is given by:*

$$J = \begin{bmatrix} \dfrac{\partial f_1}{\partial x_1} & \cdots & \dfrac{\partial f_1}{\partial x_n} \\ \vdots & \ddots & \vdots \\ \dfrac{\partial f_m}{\partial x_1} & \cdots & \dfrac{\partial f_m}{\partial x_n} \end{bmatrix}$$

Some simple examples of bifurcations occur for equilibrium points in the plane. Consider the dynamical system (2.1.1) with state-space $\mathbb{R}^2$. Suppose $x_0 \in \mathbb{R}^2$ is an equilibrium point of (2.1.1). For any set of parameters α, we consider six possible sets of eigenvalues λ_1, λ_2 of the Jacobian of f. Five of these cases occur when both eigenvalues have non-zero real part. The dynamics in these five regions are shown in Figure 2.2 and Figure 2.3. The sixth case occurs if the real part of one or both eigenvalues is zero; this is where a bifurcation occurs.

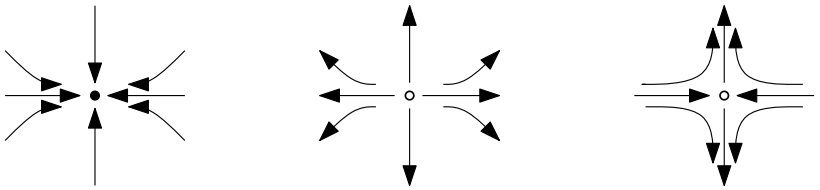

Figure 2.2: Phase portraits for equilibrium nodes in the plane. From left to right: Stable node, Unstable node, Saddle point

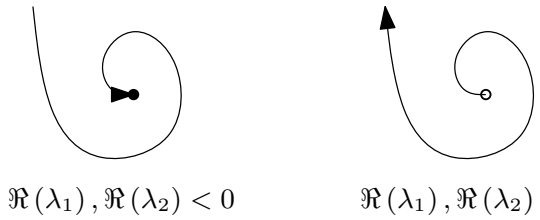

Figure 2.3: Phase portraits for equilibrium focuses in the plane. From left to right: Stable focus, Unstable focus

Now consider the dynamical system in (2.1.2). If $\alpha < 0$, then there are no equilibrium solutions in the system. Then consider the other two cases:

1. If $\alpha = 0$

   $$J|_{(0,0)} = \begin{bmatrix} 0 & 0 \\ 0 & -1 \end{bmatrix}$$

   The associated eigenvalues are $\lambda_1 = 0$ and $\lambda_2 = -1$.

2. If $\alpha > 0$:

   $$J|_{(\sqrt{\alpha},0)} = \begin{bmatrix} -2\sqrt{\alpha} & 0 \\ 0 & -1 \end{bmatrix}$$

   The associated eigenvalues are $\lambda_1 = -2\sqrt{\alpha}$ and $\lambda_2 = -1$

   $$J|_{(\sqrt{\alpha},0)} = \begin{bmatrix} 2\sqrt{\alpha} & 0 \\ 0 & -1 \end{bmatrix}$$

   The associated eigenvalues are $\lambda_1 = 2\sqrt{\alpha}$ and $\lambda_2 = -1$

Hence we can create a 1-dimensional bifurcation diagram for this system as shown in Figure 2.4. This type of a bifurcation is called a **saddle-node** bifurcation.

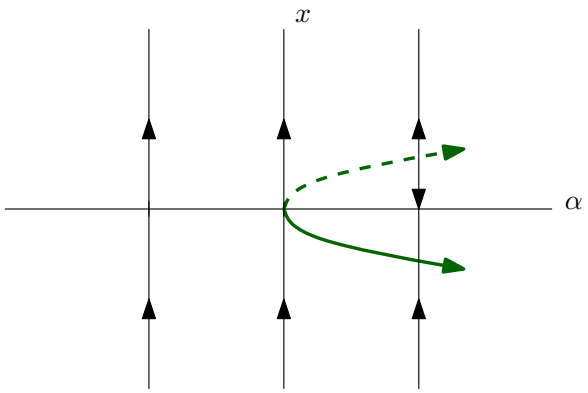

Figure 2.4: The Bifurcation diagram consists of the $\alpha - axis$ with bifurcation point at $\alpha = 0$, the x axis and the green line indicating the two equilibrium solutions are for clarity.

Therefore a co-dimension 1 bifurcation of an equilibrium point occurs either when the real part of only one eigenvalue or only a pair of conjugate eigenvalues of the Jacobian is equal to zero. For periodic orbits we can similarly define a condition for the bifurcation points as we did above for equilibrium points using the Jacobian. To do that we need to first introduce some more definitions. Let $x(t)$ be a periodic solution of (2.1.1), with period T. Consider a small perturbation from this periodic solution given by:

$$v(t) = x(t) + \xi(t) \tag{2.1.3}$$

Substituting (2.1.3) into (2.1.1) and ignoring $O\left(\|\xi\|^2\right)$ we get the following system of equations:

$$\dot{\xi}(t) = J\xi(t) \tag{2.1.4}$$

Where J is the Jacobian of f. This is the variational system associated with (2.1.1). This leads to the following definition.

Definition 2.12. *Let $x(t)$ be a periodic solution of (2.1.1) and period T. Let J be the Jacobian of f then the **Monodromy** matrix, M, of $x(t)$ at $x(0)$ is given by $Y(T)$,*

where Y satisfies the following initial value problem:

$$\dot{Y}(t) = JY(t) \quad , \quad Y(0) = \mathbb{I}_{n\times n} \tag{2.1.5}$$

The Monodromy matrix is non-singular and any solution, $\xi(t)$ to (2.1.4) will satisfy:

$$\xi(T) = M\xi(0) \tag{2.1.6}$$

From this property it follows that the Monodromy matrix plays an analogous role (for periodic solutions) as the Jacobian of f (for equilibrium solutions). In particular the linear stability of a perturbation at $x(0)$ of the periodic solution depends on the modulus of the eigenvalues of $Y(T)$.

The eigenvalues of $Y(T)$ are called **Floquet multipliers**. A linear perturbation in the direction of an eigenvector associated with an eigenvalue in the interior of the unit circle would result in a trajectory which asymptotically approaches the periodic orbit. On the other hand a linear perturbation in the direction of an eigenvector associated with an eigenvalue in the exterior of the unit circle would result in a trajectory which moves away from the periodic orbit. Finally the Monodromy matrix of a periodic orbit will always contain a trivial eigenvalue equal to 1. This eigenvalue is associated with the direction of the flow at the starting point of the orbit.

Another concept which is fundamental to the study of periodic orbits in dynamical systems is that of a Poincaré map. Let $x(t)$ be a periodic solution (2.1.1) with period T. Suppose also that the state-space is $\mathbb{R}^n$ and the flow of the system is given by ϕ^t. Then we can find an $n-1$ dimensional surface containing $x(0)$, Σ, which is transverse to the flow f i.e. $f(x)\cdot n(x) = 0$ for all points $x \in \Sigma$, where $n(x)$ is the normal vector. Furthermore we can find an open neighborhood, $V \subset \Sigma$ of $x(0)$ such that all points $y \in V$, there exists a minimal $\tau_y \approx T$ with $\phi^{\tau_y}(y) \in \Sigma$. Then we can write a discrete map, P, as described in Figure 2.5, known as the **Poincaré map** as follows:

$$P : V \to \Sigma$$

$$y \mapsto \phi^{\tau_y}(y)$$

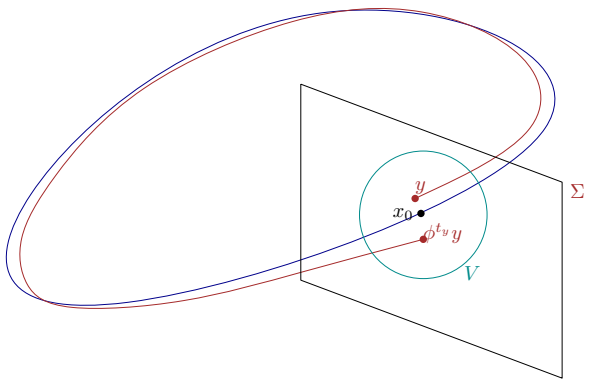

Figure 2.5: Poincaré Map Illustration

We can analogously define bifurcations for discrete maps as we did above for continuous-time dynamical systems. Note that a periodic orbit becomes a fixed point of a the associated Poincaré map. Hence the problem of studying the bifurcations of time-continuous periodic solution can be turned into one of studying fixed points of discrete dynamical systems. The role played by the eigenvalues of the Jacobian are replaced by Floquet multipliers of the periodic solution at the initial point. In the case of the equilibrium solution the dynamics is decided by whether eigenvalues have positive or negative real part. In the case of periodic orbits we are interested in whether the Floquet multipliers are inside or outside the unit circle.

2.2 Normal Forms

The normal form of a dynamical system is in a sense the "simplest" form that the system of differential equations can be written in. It is a local description, in that a normal form for a dynamical system is necessarily valid only for a neighborhood (in parameter space and phase space) of an equilibrium or fixed point . We can use the theory of normal forms to also study periodic solutions through the use of Poincaré maps. First we need to define some notation. Let

$$P_k = span\left\{ x_1^{a_1} ... x_n^{a_n} \middle| \sum_{i=1}^{n} a_i = k \right\}$$

We can then define

$$H_k = \underbrace{P_k \times ... \times P_k}_{\text{n times}}$$

and set:

Now consider the system of differential equations given by (2.1.1), with a fixed point at the origin (we can always translate the fixed point to the origin). Let the Jordan canonical form of the Jacobian of f at the origin be given by J. Then through a linear transformation we can write:

$$\dot{x} = Jx + F_2(x) + ...F_{r-1}(x) + \mathcal{O}(|x|^p) \tag{2.2.1}$$

Then we apply the transformation $x \mapsto y + h_2(y)$ to (2.2.2), where $h_2(y) \in H_2$ and has not yet been fixed. we can then rewrite (2.2.2) in the form:

$$\begin{aligned}\dot{x} &= J(y + Jh_2(y)) + F_2(y + h_2(y)) + \mathcal{O}\left(|y|^3\right) \\ &= Jy + Jh_2(y) + F_2(y) + \mathcal{O}\left(|y|^3\right)\end{aligned}$$

On the other hand we have:

$$\begin{aligned}\dot{x} &= (y + \dot{h}_2(y)) \\ &= \dot{y} + Dh_2(y)\dot{y} \\ &= (id + Dh_2(y))\,\dot{y}\end{aligned}$$

So that we have:

$$(id + Dh_2(y))\,\dot{y} = Jy + Jh_2(y) + F_2(y) + \mathcal{O}\left(|y|^3\right)$$

Now for a sufficiently small neighborhood of $y = 0$, the matrix $(id + Dh_2(y))$ is invertible. Furthermore we can expand it in the form:

$$(id + Dh_2(y))^{-1} = id - Dh_2(y) + \mathcal{O}\left(|y|^2\right)$$

Hence we can write:

$$\begin{aligned}\dot{y} &= (id + Dh_2(y))^{-1} Jy + Jh_2(y) + F_2(y) + \mathcal{O}\left(|y|^3\right) \\ &= Jy + Jh_2(y) + F_2(y) - Dh_2(y)Jy + \mathcal{O}\left(|y|^3\right)\end{aligned}$$

Ideally we want to eliminate the term $F_2(y)$ and we would choose $h_2(y)$ accordingly. Although $F_2(y) \in H_2$, it does not follow that for some $h_2 \in H_2$ we have:

$$F_2(y) = Dh_2(y)Jy - Jh_2(y)$$

However given an arbitrary function $h_j \in H_j$ we can define the following notation:

$$L_J(h_j) = Dh_j(y)Jy - Jh_j(y)$$

Then can consider the space $L_J(H_2)$ and choose $h_2(y)$ in such a way that $\tilde{F}_2(y) = F_2(y) - L_J(h_2(y))$ is orthogonal to $L_J(H_2)$. Note that Jy and $\tilde{F}_2(y)$ would be invariant under a new transformation $y \mapsto z + h_3(z)$. Thus we can then follow the same process to iteratively get the following theorem.

Theorem 2.1 (**Normal Form Theorem**). *By a sequence of analytic coordinate changes of the form:*

$$x \mapsto x + h_j(x)$$

and a linear change of co-ordinates, we can transform (2.2.2) to the form

$$\dot{y} = Jx + \tilde{F}_2(y) + ...\tilde{F}_{p-1}(y) + \mathcal{O}\left(|y|^p\right) \tag{2.2.2}$$

where $\tilde{F}_k$ is orthogonal to $L_J(H_k)$

Consider for example a 2-dimensional dynamical system with independent variables x and y and parameter $\alpha \in \mathbb{R}$. Suppose there is an equilibrium solution at the $(0, 0)$ with parameter value $\alpha = 0$. Suppose also that at the equilibrium the Jacobian has two non-zero imaginary eigenvalues given by $\lambda(0) = \pm i\omega(0)$. Then we can find a linear

transformation such that the Jacobian at the origin takes the form:

$$\begin{pmatrix} \Re\left(\lambda\left(\alpha\right)\right) & -\Im\left(\lambda\left(\alpha\right)\right) \\ \Im\left(\lambda\left(\alpha\right)\right) & \Re\left(\lambda\left(\alpha\right)\right) \end{pmatrix} =$$

We can then write $\lambda(\alpha)$, for a neighborhood of $\alpha = 0$, as:

$$\lambda(\alpha) = \left\|\lambda\left(\alpha\right)\right\| e^{2\pi i\theta(\alpha)}$$

So that we can write a Taylor expansion of the system in the form:

$$\begin{pmatrix} \dot{x} \\ \dot{y} \end{pmatrix} = |\lambda(\alpha)| \begin{pmatrix} \cos\left(2\pi\theta\left(\alpha\right)\right) & -\sin\left(2\pi\theta\left(\alpha\right)\right) \\ \sin\left(2\pi\theta\left(\alpha\right)\right) & \cos\left(2\pi\theta\left(\alpha\right)\right) \end{pmatrix} \begin{pmatrix} x \\ y \end{pmatrix} + \begin{pmatrix} f^1(x,y,\alpha) \\ f^2(x,y,\alpha) \end{pmatrix} \tag{2.2.3}$$

Where f^1, f^2 contain terms of order 2 or higher. We have written a dependence on α in here which should be justified. What we have implied is that there exists a bifurcation set, so that for some neighborhood of α the origin is a fixed point and the rest of the analysis is done on that neighborhood. Henceforth we omit writing the dependence of the λ and θ on α. Then through the following transformation into the complex numbers:

$$\begin{pmatrix} z \\ \overline{z} \end{pmatrix} = \begin{pmatrix} 1 & i \\ 1 & -i \end{pmatrix} \begin{pmatrix} x \\ y \end{pmatrix}$$

We get the following equivalent system

$$\begin{pmatrix} \dot{z} \\ \dot{\overline{z}} \end{pmatrix} = |\lambda| \begin{pmatrix} e^{2\pi i\theta} & 0 \\ 0 & e^{2\pi i\theta} \end{pmatrix} \begin{pmatrix} z \\ \overline{z} \end{pmatrix} + \begin{pmatrix} F^1(z,\overline{z},\alpha) \\ F^2(z,\overline{z},\alpha) \end{pmatrix}$$

With F^1 and F^2 conjugate functions of f^1 and f^2. That is to say we can transform (2.2.3) to the system:

$$\dot{z} = |\lambda| e^{2\pi i\theta} z + F^1(z,\overline{z},\alpha)$$

Now after calculating $L_J\left(H_2\right), L_J\left(H_3\right),$ and $L_J\left(H_4\right)$, we find that F_2^r, F_4^r must

be zero. This is because $L_J H^2$ and $L_J H^3$ have the same dimension as H^2 and H^3. Further F_3^r must have the form $c(\alpha)z^2\overline{z}$. That is the normal form as prescribed in Theorem 2.1 for (2.2.3) is given by:

$$\dot{z} = \lambda(\alpha)z + c(\alpha)z^2\overline{z} + \mathcal{O}\left(z^5\right)$$

Or in polar co-ordinates we get:

$$\begin{aligned}\dot{r} &= \mu r + ar^3 + \mathcal{O}\left(r^5\right)\\ \dot{\theta} &= \omega + br^2 + \mathcal{O}\left(r^4\right)\end{aligned}$$

Where $\lambda(\alpha) = \mu(\alpha) + i\omega(\alpha)$ and $c(\alpha) = a(\alpha) + ib(\alpha)$. We can now Taylor expand the above around $\alpha = 0$ since it is valid for a neighborhood of $\alpha = 0$. That expansion will be given by:

$$\begin{aligned}\dot{r} &= \mu'(0)\alpha r + a(0)r^3 + \mathcal{O}\left(\alpha^2 r, \alpha r^3, r^5\right)\\ \dot{\theta} &= \omega(0) + \omega'(0)\alpha + b(0)r^2 + \mathcal{O}\left(\mu^2, \mu r^2, r^4\right)\end{aligned} \tag{2.2.4}$$

The dynamics around this point are entirely determined by $\mu'(0)$ and $a(0)$. At the point where $\alpha = 0$, a Hopf bifurcation occurs. If $\mu'(0)a(0) > 0$, then a periodic orbit appears as we go from $\alpha > 0$ to $\alpha < 0$. On the other hand if $\mu'(0)a(0) < 0$ then a periodic solution appears as we go from $\alpha < 0$ to $\alpha > 0$. The associated periodic orbit in each case is stable if $a < 0$ and unstable if $a > 0$. The former is called a super-critical bifurcation and the latter a sub-critical bifurcation. We give an example of one of four possible scenarios in Figure 2.6.

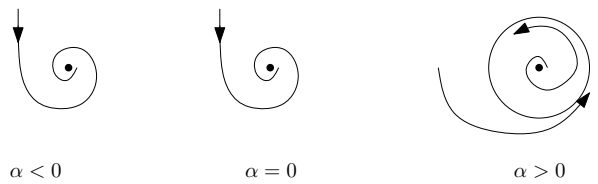

Figure 2.6: Phase portraits of a super-critical Hopf-Bifurcation with $\mu'(0) > 0$ and $a(0) < 0$

The reason we study this 2-dimensional normal form is because it is applicable whenever exactly two eigenvalues of the Jacobian are non-zero and imaginary (or in the case of maps two non-real Floquet multipliers with modulus 1). The application comes through the theory of center manifolds. We introduce the following definitions to motivate this concept.

Definition 2.13. *Consider a fixed point x_0 of (2.2.2), with Jacobian J at that point. The **stable**, **unstable**, **center** invariant spaces, denoted $E^u, E^s,$ and $, E^c,$ are the eigenspaces associated with eigenvalues which have real part less than zero, greater than zero, and equal to zero respectively.*

We can give a similar definition for Poincaré maps.

Definition 2.14. *Consider periodic solution $x(t)$ of (2.2.2). Let M be the associated monodromy matrix, M, at $x(0)$. The **stable**, **unstable**, **center** invariant spaces, denoted $E^u, E^s,$ and $, E^c,$ are the eigenspaces associated with Floquet multipliers which have modulus less than 1, greater than 1, and equal to 1 respectively.*

Further near the equilibrium point or fixed point we can also locally define the **stable manifold**, W^s, and the **unstable manifold**, W^u. The manifolds represent the orbits which are exponentially approach or move away from the equilibrium point. The invariant spaces E^s and E^u are tangent to W^s and W^u, respectively, at the point x_0 for continuous-time systems and $x(0)$ for Poincaré maps. We can also define the **center manifold**, W^c which represents those orbits whose dynamics are not determined by the stable and unstable manifolds. E^c is the tangent space of the center manifold at the point x_0 for continuous-time systems and $x(0)$ for Poincaré maps. This means through the method of center manifold reduction we restrict ourselves only to those eigenvalues (Floquet Multipliers) which have zero real part (modulus 1). We know that the dynamics around the bifurcation point are essentially captured by the dynamics around the bifurcation point restricted to the center manifold. For example consider a dynamical system where the Jacobian has exactly two eigenvalues with zero real part and non-zero imaginary part. Suppose it also has any number of eigenvalues with non-zero real part. When we restrict this system to the center manifold then the normal form will be given by (2.2.4). Then by calculating the normal form coefficients we can infer the dynamics around that point in the center manifold. If we know the dynamics in the center manifold then we know the dynamics around

that point.

2.3 LPNS Bifurcation

The LPNS bifurcation is a co-dimension two bifurcation for periodic orbits where a Limit Point of Cycle (LPC) bifurcation set intersects a Neimark-Sacker (NS) bifurcation set. It is a bifurcation point of the associated Poincaré map for the periodic solution. Here we describe the dynamics around each of these bifurcations.

We have already encountered the an analogue of the LPC bifurcation in Section 2.1 for equilibria: the saddle-node bifurcation. A LPC bifurcation for equilibrium points occurs when an eigenvalue of the Jacobian at that point is zero. For periodic orbits a LPC bifurcation occurs when one of the Floquet multipliers is equal to $+1$. In the case of equilibrium points we see the appearance/disappearance of two equilibrium points whereas for periodic orbits we see the appearance/disappearance of two periodic orbits. If we were to associate each periodic orbit with a fixed point of the Poincaré map, P, then one possible set of phase portraits in the neighborhood of the LPC bifurcation are as in Figure 2.7.

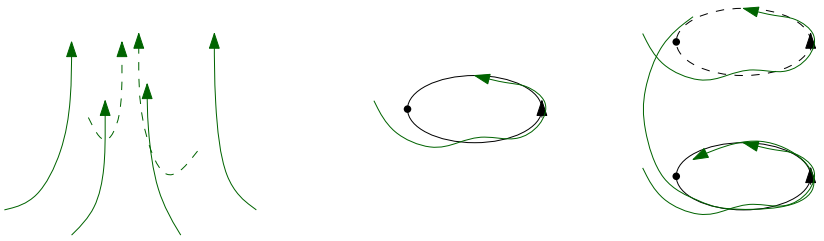

Figure 2.7: Phase portraits for a Limit-Point of Cycle bifurcation

We have also encountered an analogue of the NS bifurcation for equilibria: the the Hopf bifurcation. A NS bifurcation occurs when the modulus of two complex conjugate Floquet multipliers is equal to 1. This signals the appearance/disappearance of a closed invariant set from the Poincaré map. That is to say it is associated with the appearance/disappearance of a 2D invariant tours in the dynamical system. The

phase portraits around this kind of a bifurcation are shown in Figure 2.8 for varying associated Floquet multipliers.

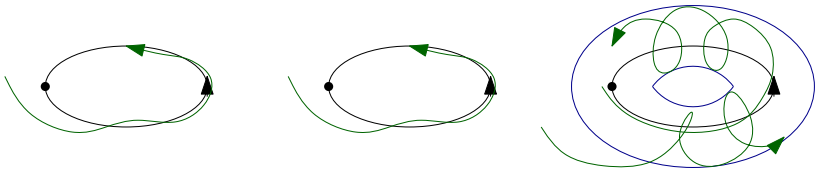

Figure 2.8: Phase portraits for a Neimark-Sacker Bifurcation

It is tempting to assume that the dynamics around the LPNS bifurcation are the same as those of a Saddle-Node Hopf bifurcation for a fixed point. The dynamics of such a system are described in [15]. However there is a complication. A torus is topologically equivalent to $S^1 \times S^1$. An orbit on the torus can be of one of two kinds. First it can be space filling curve covering every point of the torus eventually. Second if the ratio of the periods along each of the axis of the torus is rational, then the orbit will be periodic. Since there are countably many rationals between any two distinct real numbers, then this will happen infinitely often for any continuous variation of parameters. This type of appearance of periodic orbits is called resonance and it affects the dynamics in complicated ways that are not present in the Saddle-Node Hopf bifurcation. If the ratio is 1:1, 1:2, 1:3, or 1:4 it is called strong resonance. The reason for this distinction is that strong resonances affect the dynamics in much more complicated ways than non-strong resonances. Around strong resonances we may not have the appearance of the invariant torus at all.

In the absence of strong resonances we can still find vastly different dynamics. The parameter values on which the LPNS bifurcation occurs is of course on a curve of Neimark-Sacker bifurcation. On any neighborhood of the LPNS bifurcation on the Neimark-Sacker bifurcation there will be an infinite number of periodic orbits forming through resonances. As the contribution of the higher order terms increase, the region in which the periodic orbits exist will exponentially grow. This phenomenon is called

Arnold Tongues and is shown in Figure 2.9. For non-strong resonances these regions grow much slower as a function of the contribution of the higher order terms. This is one reason why we can bypass the existence of non-strong resonances near the LPNS bifurcation.

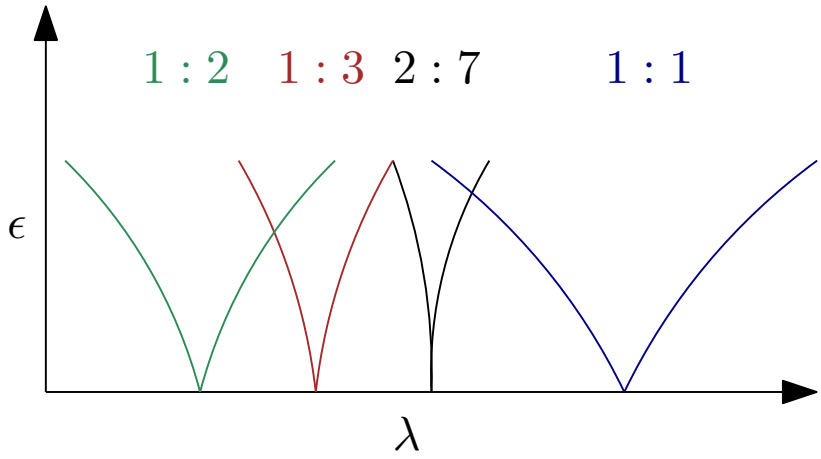

Figure 2.9: The phenomenon of Arnold Tongues. λ-axis represents a Neimark-Sacker bifurcation curve. ϵ represents the contribution of higher-order terms, with no contribution at the λ-axis. Non-strong resonances have "thinner" tongues, and hence they are more negligible. Note that infinitely many tongues always exist any neighborhood, but we can not show all of them.

.

The normal form of the LPNS bifurcation, derived by De Witte, is given by:

$$\begin{aligned}
\frac{d\tau}{dt} &= 1 - \xi_1 + \alpha_{200}\xi_1^2 + \alpha_{011}\left|\xi_2\right|^2 + \alpha_{300}\xi_1^3 + \alpha_{111}\xi_1\left|\xi_2\right|^2 + \dots \\
\frac{d\xi_1}{d\tau} &= a_{200}\xi_1^2 + a_{011}\left|\xi_2\right|^2 + a_{300}\left|\xi_1\right|^3 + a_{111}\xi_1\left|\xi_2\right|^2 + \dots \\
\frac{d\xi_2}{d\tau} &= i\omega\xi_2 + b_{110}\xi_1\xi_2 + b_{210}\xi_1^2\xi_2 + b_{021}\xi_2\left|\xi_2\right|^2 + \dots
\end{aligned} \tag{2.3.1}$$

These sets of equations represent the center-manifold on as we travel along the periodic orbit. Here ξ_1 is a real coordinate while ξ_2 is a complex coordinate. Note that τ does not appear in the equations describing ξ and ξ_2. Therefore we can decouple the motion along the orbit from motion transverse to it. So that the center manifold is smoothly orbitally equivalent to a simpler system where the equations for transverse

coordinates are as follows:

$$\begin{aligned}\frac{d\xi}{d\tau} &= \beta_1 + \xi^2 + s\left|\zeta\right|^2 + \mathcal{O}\left(\left|\left(\xi,\zeta,\overline{\zeta}\right)\right|^4\right)\\ \frac{d\zeta}{d\tau} &= \left(\beta_2 + i\omega_1\right)\zeta + \left(\theta + i\vartheta\right)\xi\zeta + \xi^2\zeta + \mathcal{O}\left(\left|\left(\xi,\zeta,\overline{\zeta}\right)\right|^4\right)\end{aligned} \tag{2.3.2}$$

Where ξ is a real co-ordinate while ζ is a complex coordinate. This system is similar to that of the Saddle-Node Hopf bifurcation [15]. The system can be simplified using cylindrical co-ordinates (ignoring higher order terms) into the form:

$$\begin{aligned}\frac{d\xi}{d\tau} &= \beta_1 + \xi^2 + s\rho\\ \frac{d\rho}{d\tau} &= \rho\left(\beta_2 + \theta\xi + \xi^2\right)\end{aligned} \tag{2.3.3}$$

Here $\xi \in \mathbb{R}$ and $\rho = \|\zeta\|^2$. One possible unfolding of this system (with possible time reversal) is shown in Figure 2.10. β_1 and β_2 form the axis of the bifurcation diagram and are the same variables as in (2.3.3). For each section of the bifurcation diagram a phase portrait is also displayed. In the phase portraits the horizontal axis represents ξ and the vertical component represents ρ. The phase portraits are time periodic as prescribed by $d\tau/dt$ above, but we see the solution at one given time. Thus in the phase portraits in Figure 2.10 each circle on the horizontal axis represents a periodic orbit. Further we have ommited the angular coordinate in (2.3.3) which is also time-periodic. Thus any object off the horizontal axis also has a second period and we see the solution at one given time along that period as well. Thus a circle off the horizontal axis represents an invariant torus. Filled circles are stable invariant sets and unfilled circles are unstable invariant sets. A closed curve which is topologically equivalent to a circle in the phase portraits represents a 3-torus. S represents the LPC bifurcation. H represents the NS bifurcation. T represents the appearance/disappearance of a 3-torus. Two heteroclinic orbits connected unstable periodic orbits are shown in the diagram labeled P.

A further complication is that although the EWM does not have any terms of order 3 or higher, the normal form of it might have terms of order 3 or higher. The

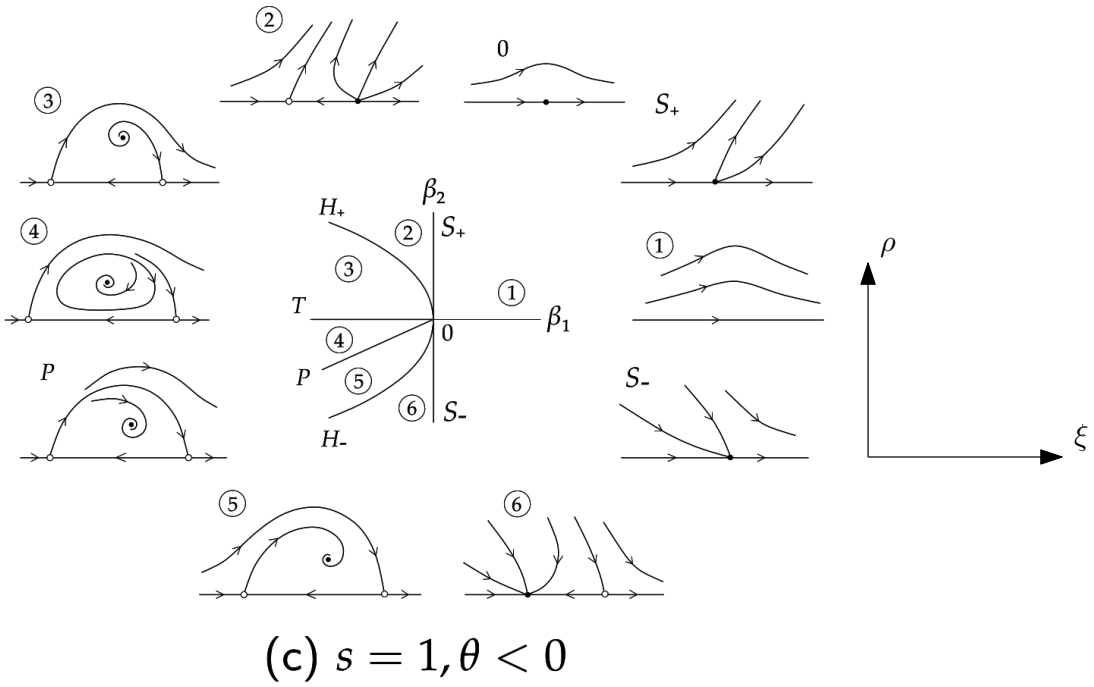

Figure 2.10: Example of unfolding for the LPNS bifurcation. This picture is taken from [4]. The bifurcation diagram is in the center. The phase portraits for the different regions of the bifurcation diagram around around the bifurcation diagram. The axis on the right is for the phase portraits.

unfolding shown in Figure 2.10 may further be complicated by these terms as is the case in the Fold-Flip bifurcation discussed in [14]. Consider for example the heteroclinic connection between the two periodic orbits labeled P in Figure 2.10. The effect of the higher order terms will generically be that the unstable manifold and the stable manifolds will not intersect tangentially and instead intersect transversely. In that case we expect to may find a "tangle" of heteroclinic orbits as shown in Figure 2.11. Due to these higher order terms we also expect to see other interesting structures such as homoclinic orbits for each of the periodic solutions. This "tangle" going between one unstable manifold and back to the other should be reminiscent of the discussion in Section 1.5.1.

2.4 Results of Bifurcation Analysis

The results presented in this section are from computation in MatCont. MatCont is a software package for MATLAB [5]. There is both a GUI and command line version.

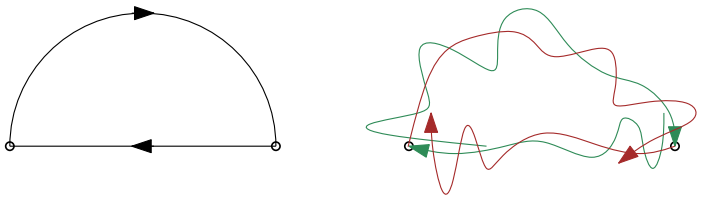

Figure 2.11: On the left we have the heteroclinic connections between our two unstable periodic orbits as shown in Figure 2.10. On the right we show the possible effects of higher order terms. The unstable manifold (brown) of each periodic orbit transversely intersects with the stable manifold (green) of the other periodic orbit. Thus each pair of manifolds "tangles". For more information regarding these dynamics refer to [14].

It is a numerical tool for studying dynamical systems and bifurcations. MatCont can detect codimension 1 and codimension 2 bifurcations of both equilibria and fixed points. MatCont works by starting with an initial solution which satisfies the required conditions and then calculates a parametrized curve of solutions which satisfy the required conditions. It uses a variation of a pseudo-arclength method to do this, which involves a prediction step and a correction step which are described below. Suppose we have a system of equations:

$$\begin{aligned} F_1(\vec{x}) &= 0 \\ &\vdots \\ F_n(\vec{x}) &= 0 \end{aligned} \tag{2.4.1}$$

Where $\vec{x}$ is made up of $n+1$ variables. Suppose also that $\vec{x}_0$ satisfies $F(\vec{x}_0) = 0$. We can guess that the there is a nearby solution at $\vec{x}_1^1 = \vec{x_0} + h\vec{T}_0$. The vector T_0 is first chosen arbitrarily, but after we have calculated a second solution we calculate it as the approximate tangent of the curve of solutions at that point. In order to apply a Newton correction step, we need the system (2.4.1) to have $n+1$ equations. So we add to it the equation:

$$F_{n+1}(\vec{x}) = \langle \vec{x} - \vec{x_0}, \vec{T}_0 \rangle \tag{2.4.2}$$

This ensures that the correction step is orthogonal to the prediction direction $\vec{T}_0$ as shown in Figure 2.12. Using the newton method and an initial guess of $\vec{x}_1^1$ we

can iteratively update the solution to $\vec{x}_1^2$, $\vec{x}_1^3$, ..., until we have a solution $\vec{x}_1$ which satisfies the system given by (2.4.1) along with (2.4.2) upto some specified tolerance. Thereafter we can iteratively find other solutions $\vec{x}_i$ for $i > 1$.

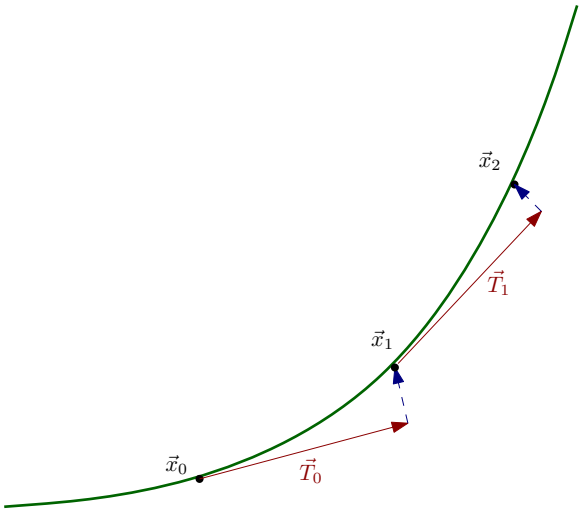

Figure 2.12: Pseudo-Arclength Method

Starting with an equilibrium or a periodic solution, we can use MatCont to detect codimension 1 bifurcations such as LPC and NS bifurcations. Using that bifurcation point we can calculate a curve of on which every point is that type of a bifurcation. Then we can detect codimension 2 bifurcations on the codimension 1 bifurcation curve. This is the method which we use to detect the LPNS bifurcation after we have found the periodic solution associated with the EWM. This system has 3 parameters: Q, α, γ. Where $Q = \frac{1}{Re}$, and α, γ are the aspect ratios.

2.4.1 Existing Results

Recall that Nagata found a periodic solution to PCF by first finding a periodic solution to TCF. Then he did a homotope to transform the periodic solution from TCF into one of PCF. A periodic solution for the EWM found using the homotopy method is discussed in [20]. van Veen begins with a periodic solution in a modified EWM and then homotopes that solution to a solution of the EWM. The modified EWM is

different from 1.5.9 in only two equation shown below:

$$\frac{da_3}{dt} = (1 - H_1)\left(\frac{L_3}{Re}a_k + a^T S_3 a\right) + H_1\left(a_3 H_2 - (a_3)^3\right) \tag{2.4.3}$$

$$\frac{da_{14}}{dt} = (1 - H_1)\left(\frac{L_{14}}{Re}a_k + a^T S_{14} a\right) + H_1\left(a_{14} H_3 - (a_{14})^3\right) \tag{2.4.4}$$

Here H_1 is a homotopy parameter from EWM to a modified EWM system. So that when $H_1 = 0$ we recover EWM and when $H_1 = 1$ the third and fourteenth equations resemble (2.2.4). This is done so that when we continue the equilibrium solution we can detect a pitchfork bifurcation in the modified system. Following a branch at the pitchfork bifurcation we can detect a Hopf bifurcation, and following that we get a periodic solution. Then we must carefully tune Re, H_1, H_2 and H_3 so that we can continue our solution to $H_1 = 0$. This is a non-trivial process and we must use a combination of educated guesses and trial & error in order to locate a periodic solution in the EWM. This process is an analogue of the method used to find a periodic solution for PCF by Nagata [16]. It should be noted that we modified the equations governing the two roll modes in the system. The periodic solution is shown in Figure 2.13 and the parameter values at which it occurs are in Table 2.1 .

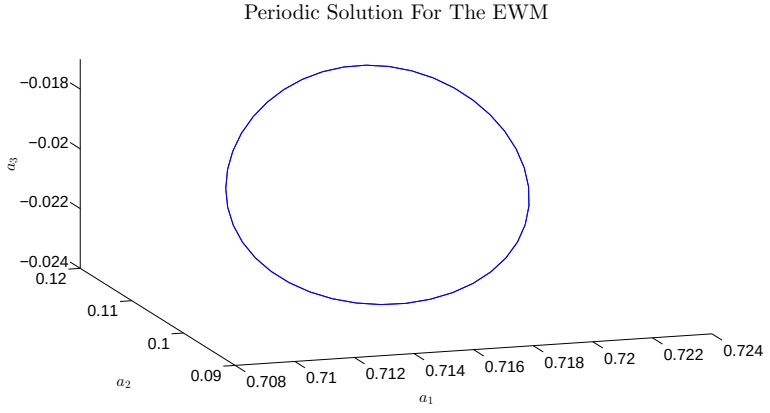

Figure 2.13: Periodic solution for the EWM

We can continue the periodic solution along the Reynolds number as $Re \to \infty$ as in the case of the periodic solution for PCF. The period seems to grow as we increase

Parameter	Values
Re	8.519577660104802e+01
α	8.663172566761049e-01
γ	1.666666666700000e+00

Table 2.1: Parameter values for the periodic solution in Figure 2.13

Re. Such a one parameter continuation of this Periodic Solution in the Extended Waleffe Model (PSEWM) along the Reynolds number leads to the detection of a LPC bifurcation and a NS bifurcation [20]. Using MatCont many such bifurcations were found as shown in Figure 2.14. These include BPC and CPC bifurcations. The BPC bifurcation is a symmetry breaking bifurcation. The periodic orbits sometimes have discrete symmetries in some co-ordinates. For example the periodic orbit shown in Figure 2.13 has the following symmetry:

$$a_4(t) = -a_4(t + T/2)$$

where T is the period of the orbit. At a BPC bifurcation we can continue to periodic solutions which dont have these symmetries. More information about these types of bifurcations can be found in [5] and [15].

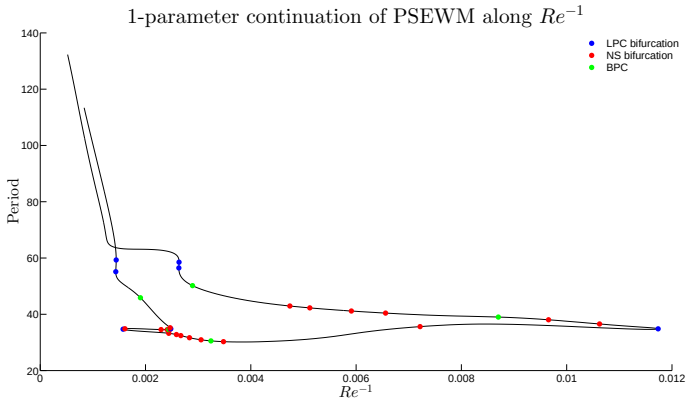

Figure 2.14: Continuation of PSEWM along Re^{-1}

2.4.2 Results

Continuing along the other two parameters, α and γ, we find two isolas of periodic solutions. These are shown in Figure 2.15 and Figure 2.16 respectively. In each case we get a closed isola of periodic solutions with many bifurcations.

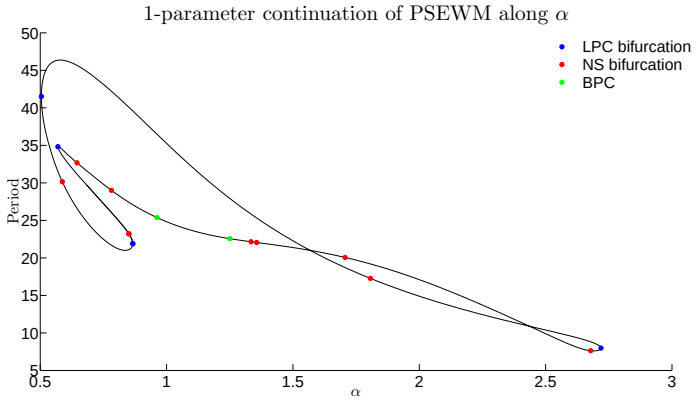

Figure 2.15: Continuation of PSEWM along α

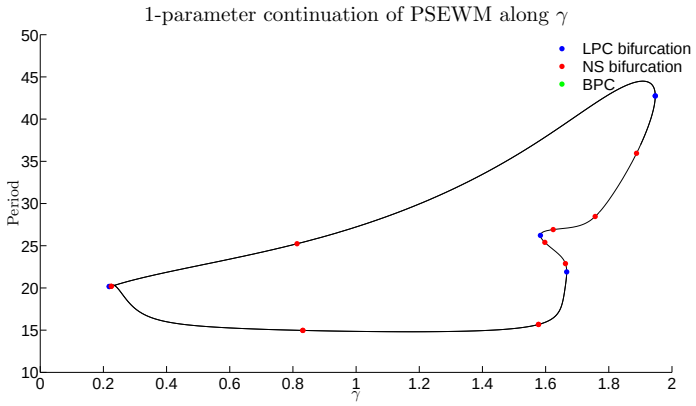

Figure 2.16: Continuation of PSEWM along γ

Using Matcont, we can also do a two parameter continuation to find curves of bifurcation points. Specifically we can calculate curves of LPC bifurcations and NS bifurcations as shown in Figure 2.17. We do not detect any periodic solutions on the outside of the outer LPC bifurcation curve, but we expect to find upto 4 periodic solutions for the same parameter value inside the inner LPC curve. This can be readily

seen from Figure 2.14. Using MatCont we can continue periodic solutions to $Re^{-1} = 0$ as in the case of PCF.

This leads to the detection of co-dimension 2 bifurcations, namely Chenciner, CPC, Resonance and LPNS. For more information on these bifurcations refer to [5] and [15]. The LPNS bifurcations occur at $Re \sim 61$ and $Re \sim 47$. The exact parameters where the LPNS bifurcations occur are shown in Table 2.2. Also in Table 2.2 we find the coefficients calculated by MatCont that we use to identify the exact type of unfolding that occurs at the bifurcation. We know the type of bifurcation because Matcont calculates the normal form coefficients. The unfolding of both of these LPNS bifurcation points is as shown in Figure 2.10. There we expect to find interesting phenomenon such as heteroclinic orbits connection two unstable periodic orbits.

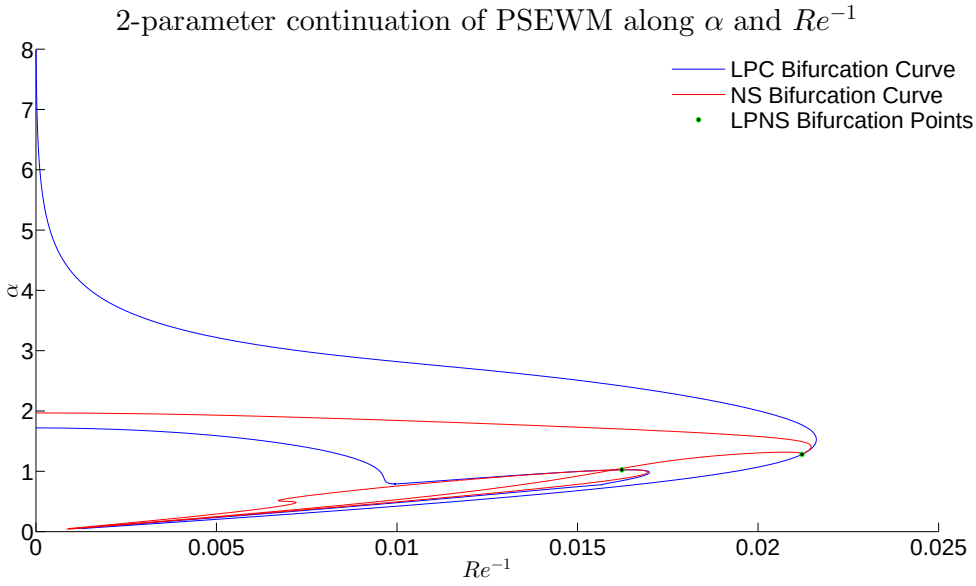

Figure 2.17: 2-Parameter continuation of PSEWM

Next we calculate an isola of periodic solutions using a 1 parameter continuation near the LPNS point at $Re \sim 61$. We choose to concentrate on this LPNS bifurcation because it occurs at a lower α value. The results are shown in Figure 2.18. As we can see the number of unstable multipliers changes by 2 when going through a NS bifurcation and by 1 when going through a LPC bifurcation.

	LPNS 1	LPNS 2
Re	6.162531590814498e+01	4.713684907128906e+01
α	1.024832250589729e+00	1.280389040171663e+00
γ	1.666666666700000e+00	1.666666666700000e+00
s	1	1
θ	-1.063337206946596e+00	-5.032738214922368e-01

Table 2.2: Parameter values where the two LPNS bifurcations occur

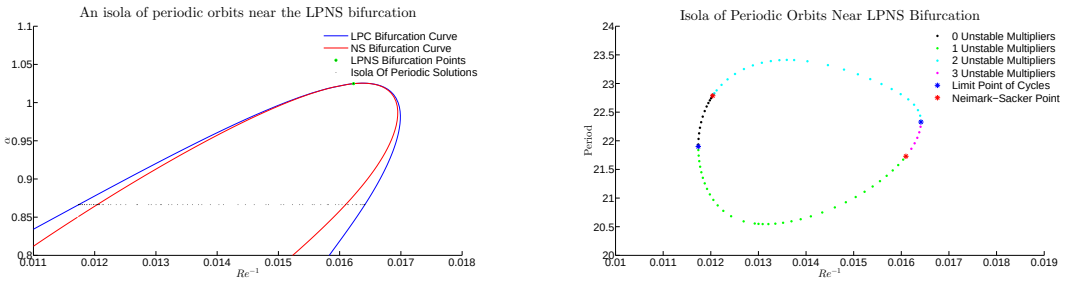

Figure 2.18: Each point on the left and the right represents a periodic solution. An isola of periodic solutions near the LPNS bifurcation is shown on the left. On the right we show the same the same isola of periodic solutions indicating the number of unstable multipliers that exist for each periodic solution.

We expect to find heteroclinic and homoclinic orbits as well as torus and 3-torus in the region where periodic orbits have 1 or 3 unstable multipliers. We can perform a crude manifold computation for periodic solutions with 1 unstable multiplier. We do this by perturbing each solution in the direction of the unique unstable eigenvector and integrate the solution. The perturbed solution almost always approaches the laminar solution, $a_i = \delta_{1i}$, after some time. One way to look for interesting orbits is to consider the root-mean-square (RMS) value of all coefficients except that of the simple laminar basis function (ϕ_1) given by:

$$RMS_{2:17} = \sqrt{a_2^2 + ... + a_{17}^2} \tag{2.4.5}$$

In most cases the $RMS_{2:17}$ value oscillates for a while and then decays to zero after sometime. We can however spot interesting orbits easily by identifying orbits where

the $RMS_{2:17}$ oscillates, and grows before (if at all) decaying. Two uninteresting orbits and two interesting orbits are shown in Figure 2.19.

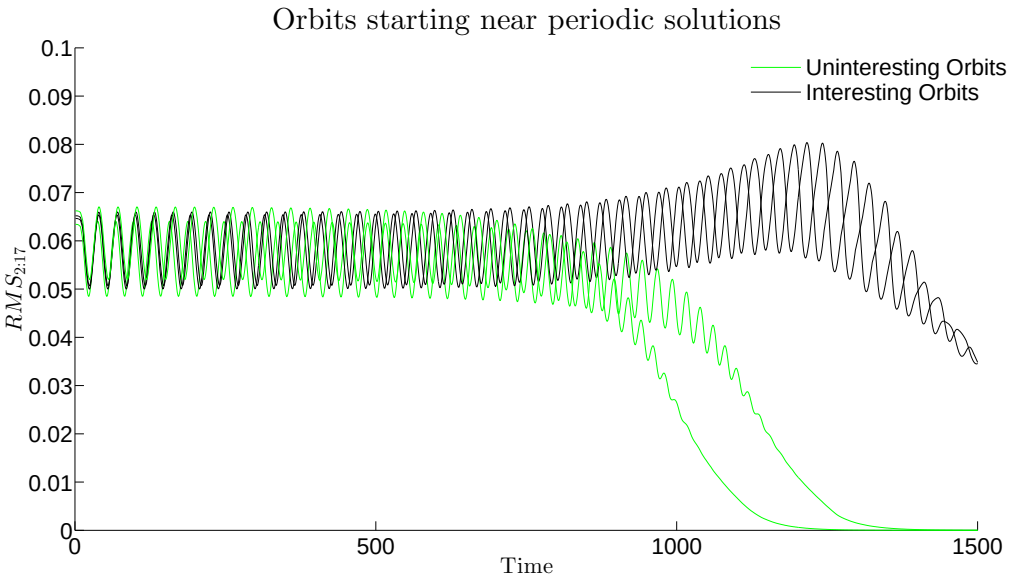

Figure 2.19: Two orbits shown in green are uninteresting because they decay to the laminar solution. $a_i = \delta_{1i}$, right away. The two orbits shown in black are interesting because the $RMS_{2:17}$ value grows before decaying. The orbits in green can be in sections of Figure 2.10 that have interesting dynamics such as heteroclinic orbits.

In the next chapter we introduce a powerful manifold computation technique and use it to search for the interesting and complicated structures shown in Figure 2.10.

Manifold Computation

The extended Waleffe model introduced in Section 1.5.2 is a low order model of PCF. In the previous chapter it was shown that this model exhibits an LPNS bifurcation. Furthermore we know that near the LPNS bifurcation we expect to find a 3-torus, heteroclinic orbits and homoclinic orbits. To explore this complex structure around the periodic solution we use a manifold computation technique devised in [21]. There in van Veen et al derive a method to examine the unstable manifold around a periodic solution. We introduce the method following that paper closely. Suppose we have a system of equations with $n+1$ independent variables and n equations. Generically we expect to find a curve of solutions for this system. In order to numerically calculate this curve from an initial solution a pseudo-arclength continuation method, as described in Section 2.4, is used. For the correction step the method uses a Newthon-Raphson algorithm. The correction step requires us to solve a linear system, $A\vec{x} = b$, and we use the method of Krylov subspace to solve this system. This type of prediction-correction method is called the Newton-Krylov method. This method is "matrix-free" since we don't explicitly use the associated matrix, A, of the linear system for the Newton-Raphson step. Rather we use the matrix-vector product $A\vec{y}$, for specified vectors $\vec{y}$.

Consider the system of differential equations (2.1.1). Suppose $x(t)$ is a periodic solution to (2.1.1). Let $\epsilon > 0$ and u be a unit vector in the unstable eigenbundle of $x(t)$ at the point $x(0)$. Suppose also there is solution $\gamma(t)$, satisfying:

$$\gamma(0) = x(0) + \epsilon u \tag{3.0.1}$$

$$g(\gamma, T) = c \tag{3.0.2}$$

for some well defined differentiable scalar function g, time T and $c \in \mathbb{R}$. This set up

is shown in Figure 3.1. We can rewrite the boundary value problem (BVP) in (3.0.1) in the form:

$$\begin{aligned} F : \mathbb{R}^{n+2} &\to \mathbb{R}^{n+1} \\ z &\mapsto (\gamma(0) - x(0) + \epsilon u, g(\gamma, T) - c) \\ &= \begin{pmatrix} 0 \\ 0 \end{pmatrix} \end{aligned}$$

Where $z = (\gamma(0), T, \epsilon)$. This means that we are solving for a BVP which is underdetermined with one degree of freedom.

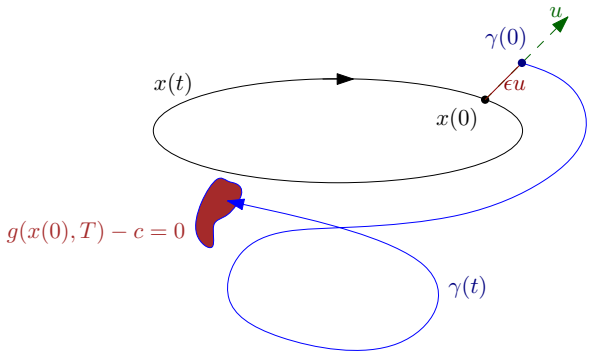

Figure 3.1: Single shooting set-up

Three functions are considered for g:

$g(\gamma, T) = T$	Solutions which have integration time c
$g(\gamma, t) = g(\gamma(T))$	Solutions which terminate at a Poincaré surface
$g(\gamma, T) = \int_0^T \lvert f(\gamma(t)) \rvert \, dt$	Solutions with fixed arclength c

Using the above set up we can now find a second solution, $\hat{z}$, which satisfies $F(\hat{z}) = 0$ for some tolerance level. We do this by first picking direction T_0 (Note that we write tangent vectors with subscripts and integration times with superscripts). We set

$\hat{z^0} = z + \Delta s T_0$, for some specified step size Δs. For the Newthon-Raphson correction step we need to solve the following:

$$\begin{aligned} \mathcal{A}\delta\hat{z}^0 &= \begin{pmatrix} DF \\ T_0 \end{pmatrix} \delta\hat{z}^j \\ &= - \begin{pmatrix} F\left(\hat{z}^0\right) \\ 0 \end{pmatrix} \end{aligned} \tag{3.0.3}$$

Then we update $\hat{z}^1 = \hat{z}^0 + \delta\hat{z}^0$. We iterate the correction step through $\hat{z}^0, \hat{z}, ..., \hat{z}^k$, with k minimal such that $F(\hat{z}$ is within a specified tolerance. If the process does not terminate after a set number of steps we can reduce the step size Δs and try again. In this we can calculate a sequence of m solutions given by $z_0 = z, z_1 = \hat{z}, z_2, ..., z_m$. The Krylov subspace method is used to solve the linear system given by 3.0.3. We can make this method (single shooting) more stable by splicing the solution γ into smaller pieces (multiple shooting). An example with γ split into 3 parts is shown in Figure 3.2.

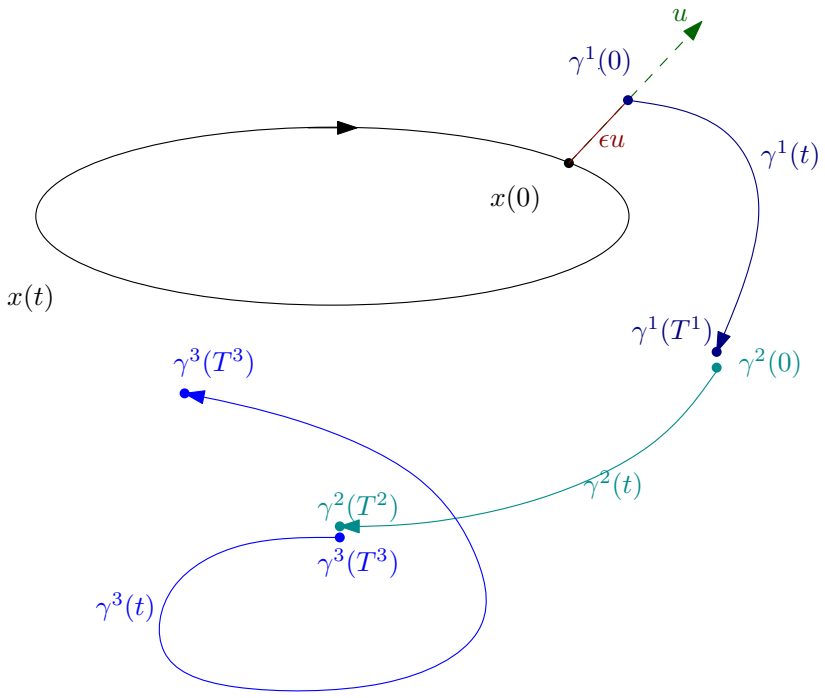

Figure 3.2: Multiple shooting example

The Newton-Krylov algorithm is the same for single and multiple shooting. However in the multiple shooting method we define z and F differently as follows:

$$z = \left(\gamma^2, ..., \gamma^k, T^1, ...T^k, \epsilon\right)$$

and

$$F(z) = \left(\gamma^2(0) - \gamma^1(T^1), ..., \gamma^k(0) - \gamma^{k-1}(T^{k-1}), g^1\left(\gamma^1, T^1\right) - c_1, ..., g^k\left(\gamma^k, T^k\right) - c_k\right)$$

With $F : \mathbb{R}^{(k-1)n+k+1} \to \mathbb{R}^{(k-1)n+k}$, so that again we have a BVP which is underdetermined by a degree of one. Where k is the number of parts that γ is broken into. $g^1, ..., g^k$ are the properties that each of the solutions must satisfy individually. Now the matrix $\mathcal{A}$ will differ based on whether we use the single shooting method or the multiple shooting method. It will also change depending on the type of function g that we use.

A simple example of a this manifold computation technique is shown in Figure 3.3. Here we shown a small section of the unstable manifold of a periodic orbit with 1 unstable multiplier. The endpoint of the orbit is chosen to end on a Poincaré section given by $a_3 = -0.022$.

3.1 Results

With the use of the crude shooting method described in the previous chapter parameter values where interesting phenomenon may occur were isolated. The manifold computation technique was used with arclength, fixed-time and varying Poincaré sections to explore the dynamics for those parameter values. In one computation we fixed a Poincaré section given by:

$$\sum_{i=2}^{17} a_i^2 = 0.055 \tag{3.1.1}$$

We report here the results which were found for parameter values shown in Table 3.1 using the above Poincaré section.

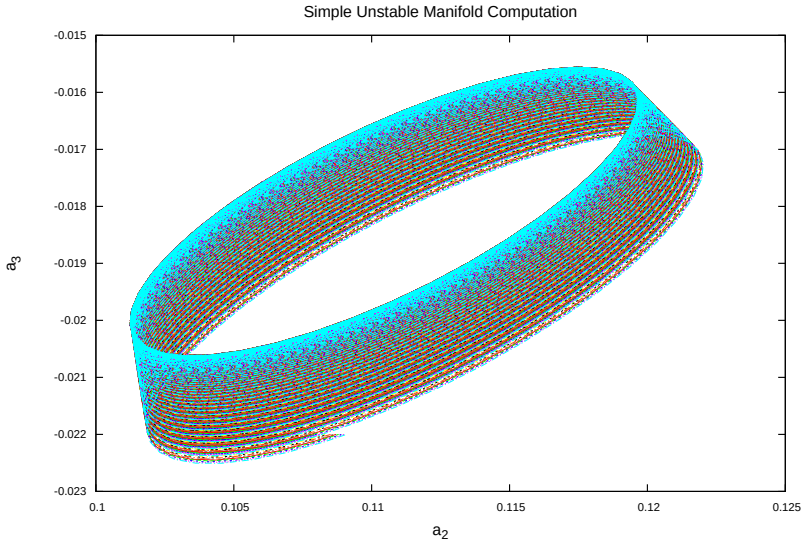

Figure 3.3: The unstable manifold of a periodic is shown here by the computation of many orbits originating near the periodic orbit. The starting point of each orbit is a perturbation of a point on the periodic orbit along the unique unstable eigenvector at that point.

Parameters	Values
Re	8.305396483288619e+01
α	8.663172655828357e-01
γ	1.666666666700000e+00

Table 3.1: Parameter values for which a quasi-periodic orbit and a homoclinic orbit were detected

We detected two interesting phenomenon, a quasi-periodic orbit and a homoclinic orbit. In order to find these results we visually represent the Poincaré section of the unstable manifold as in Figure 3.4.

In Figure 3.4, the intersection point of Periodic orbit 1 and the Poincaré section represents an orbit which originates near Periodic orbit 1 (as all other points) and terminates near the same Periodic orbit. We plot this homoclinic orbit and some nearby orbits in Figure 3.5. This homoclinic orbit is an analogue of the one discussed in Section 1.5.1.

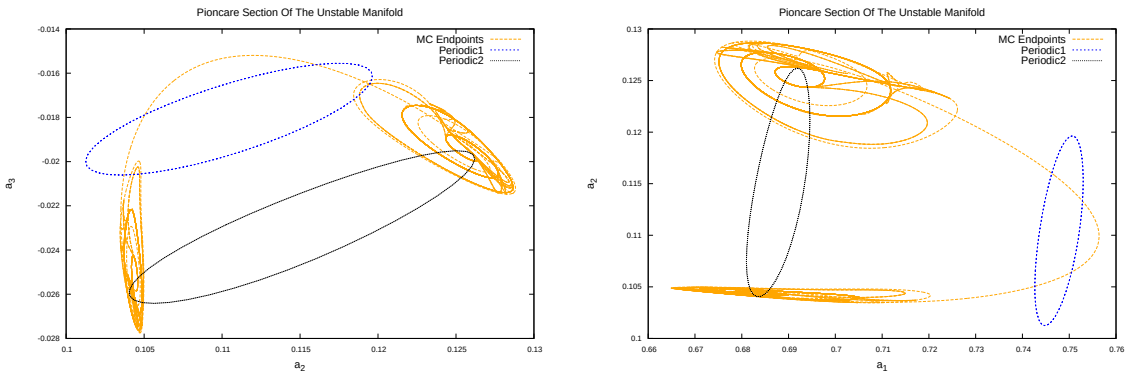

Figure 3.4: The above two figures show the Poincaré section of the unstable manifold of a periodic orbit. The orange curve represents the endpoints of many orbits which originate near the Periodic 1 and terminate at the Poincaré section described in (3.1.1). We are interested in finding orbits which terminate near Periodic 2 (possible heteroclinic orbits) and orbits which terminate near Periodic 1 (possible homoclinic orbits).

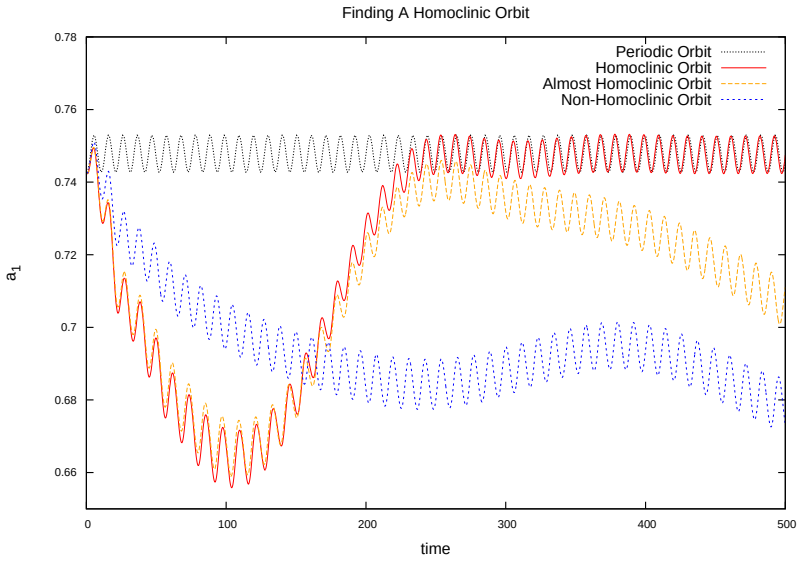

Figure 3.5: Multiple shooting example

Further we can detect a quasi-periodic orbit by searching the sections of Figure 3.4 which seem interesting. This is shown in Figure 3.6.

Thus we have found a homoclinic orbit and a quasiperiodic orbit in the EWM, the existences of where were predicted by the unfolding at the LPNS point shown in

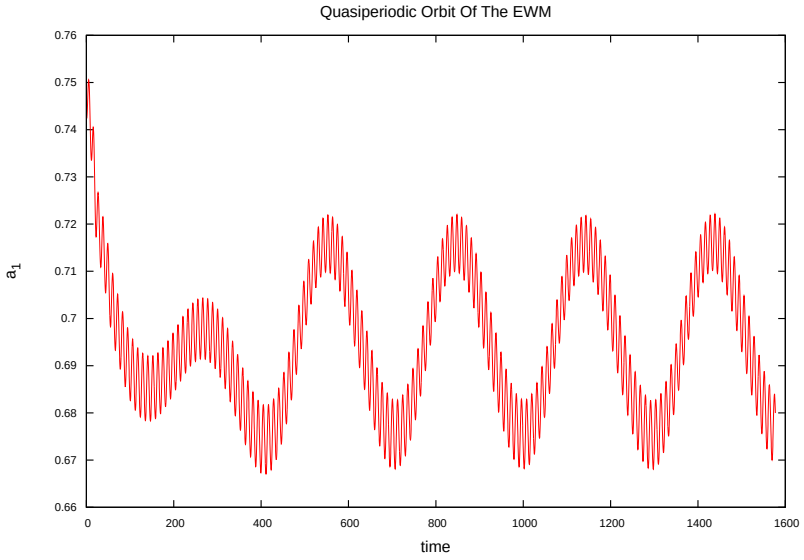

Figure 3.6: Multiple shooting example

Figure 2.10. Furthermore we have found similar homoclinic orbits and quasi-periodic solutions for other parameter values near those listed in Table 3.1. In the next chapter we discuss a method to find a parameterized family of homoclinic orbits using the initial homoclinic orbit shown in Figure 3.5.

Continuation of Homoclinic and Heteroclinic orbits

4.1 Background

Much of the material covered in this section can be found in [6] and [7]. It is restated here so that this thesis can be self-contained. Recall that at the end of Section 3.1 we had isolated a homoclinic orbit for the EWM, which is a low order model that can be used to study PCF. We had discussed in Section 1.5.1 the importance of homoclinic and heteroclinic orbits in PCF in the study of the onset of turbulence. We would like now to present a method for future work to refine these homoclinic orbits and to continue them in Re and α. The BVP described below can be implemented in AUTO, which is a software package for continuation and bifurcation of ODEs [8]. This way we can study these orbits far away from LPNS point. We can study also where in the Re, α plane they exist. The boundaries of the region for which they exist are formed by the points on which the stable and unstable manifolds intersect tangentially. We discuss a method which can be used to continue a homoclinic or heteroclinic orbit.

Consider a system of ODEs defined by:

$$\frac{du}{dt} = f(u, \alpha) \tag{4.1.1}$$

Where $f : \mathbb{R}^n \times \mathbb{R}^m \to \mathbb{R}^n$, $u \in \mathbb{R}^n$ represents the state variables and $\alpha \in \mathbb{R}^m$ represents parameter values. Let ϕ^t represent the flow generated by (4.1.1).

Let $x(t)$ be a periodic solution of (4.1.1), with period T. Recall that the monodromy matrix, M, is the solution evaluated at T, of the IVP:

$$\dot{Y}(t) = JY(t) \quad , \quad Y(0) = \mathbb{I}_{n\times n} \tag{4.1.2}$$

We can define the **adjoint monodromy matrix**, N, as the solution, evaluated at T, of the IVP:

$$\dot{Z}(t) = -J^{\dagger}Z(t) \quad , \quad Z(0) = \mathbb{I}_{n\times n} \tag{4.1.3}$$

Here we have written the transpose of J as $J^{\dagger}$ to avoid confusion with the period of the orbit. We will use this notation for the rest of this section. Hereafter M and N will represent the monodromy and the adjoint monodromy matrices of a periodic orbit at some fixed point as described above. We note that:

$$\begin{aligned}\frac{d}{dt}\left(Z^{\dagger}Y\right) &= \frac{dZ^{\dagger}}{dt}Y(T) + Z(T)\frac{dY^{\dagger}}{dt} \\ &= Z^{\dagger}\left(-J^{\dagger}\right)Y + Z^{\dagger}JY \\ &= 0\end{aligned}$$

and since $Z(0)^{\dagger}Y(0) = \mathbb{I}_{n\times n}$ then we conclude that in fact $M = \left(N^{\dagger}\right)^{-1}$.

From this we can also conclude something interesting about the eigenvalues and eigenvectors of the matrices M and N, hereafter referred to as the Floquet multipliers of M and N. This is to allude to the fact that these eigenvalues represent stable perturbations when they are within the unit circle and unstable perturbations when they are outside the unit circle. Both M and N will always have a trivial eigenvalue equal to 1 by construction of the monodromy matrix and the adjoint monodromy matrix. We will show below that an eigenvector of N that has an unstable Floquet multiplier is orthogonal to to stable manifold of $x(t)$ at $x(0)$. Similarly we will show that an eigenvector of N that has a stable Floquet multiplier is orthogonal to the stable manifold of $x(t)$ at $x(0)$.

Suppose that v is an eigenvector of M with a floquet multiplier $\lambda \neq 0$ then:

$$
\begin{aligned}
& Mv = \lambda v \\
\iff & (Mv)^\dagger = \lambda v^\dagger \\
\iff & v^\dagger M^\dagger = \lambda v^\dagger \\
\iff & v^\dagger \left(\left(N^\dagger \right)^{-1} \right)^\dagger = \lambda v^\dagger \\
\iff & v^\dagger N^{-1} = \lambda v^\dagger \\
\iff & \lambda^{-1} v^\dagger = v^\dagger N
\end{aligned}
$$

The above argument can also be used to show that:

$$Nv = \lambda v \iff \lambda^{-1} v^\dagger = v^\dagger M$$

Furthermore the eigenvectors of M and N have some interesting properties that we will now explore. Consider two vectors ω and ν such that:

$$
\begin{aligned}
M\omega = \lambda_\omega \omega \quad , \quad 0 < \|\lambda_\omega\| \leq 1 \\
N\nu = \lambda_\nu \nu \quad , \quad 0 < \|\lambda_\nu\| < 1
\end{aligned}
$$

Then by using $M = \left(N^\dagger \right)^{-1}$ and the properties of eigenvectors we have the following:

$$
\begin{aligned}
\omega^\dagger \nu &= \nu^\dagger \left(N^\dagger \right)^{-1} N^\dagger \omega \\
&= \nu^\dagger M N^\dagger \omega \\
&= \nu^\dagger M \left(\omega N^\dagger \right)^\dagger \\
&= \frac{1}{\lambda_\nu} \nu^\dagger \left(\frac{1}{\lambda_\omega} \omega^\dagger \right)^\dagger \\
&= \frac{1}{\lambda_\nu \lambda_\omega} \nu^\dagger \omega
\end{aligned}
$$

Taking the absolute value of both sides we get:

$$\begin{aligned}\left|\omega^\dagger\nu\right| &= \left|\frac{1}{\lambda_\nu\lambda_\omega}\nu^\dagger\omega\right| \\ &= \frac{1}{|\lambda_\nu|\,|\lambda_\omega|}\left|\nu^\dagger\omega\right|\end{aligned}$$

But by construction $|\lambda_\nu|\,|\lambda_\omega| < 1$. Therefore we must have $\nu^\dagger\omega = 0$. That is ν and ω must be orthogonal. A similar argument can be made for the case:

$$\begin{aligned} M\omega = \lambda_\omega\omega \quad &, \quad \|\lambda_\omega\| \geq 1 \\ N\nu = \lambda_\nu\nu \quad &, \quad \|\lambda_\nu\| > 1 \end{aligned}$$

to show that ω and ν are orthogonal. We are now ready to describe the method which can be used to continue certain homoclinic and heteroclinic orbits.

4.2 Setup

Given the following system of ODEs in (4.1.1). Suppose $x^\pm(t)$ are two (not necessarily distinct) periodic solutions of (4.1.1) with periods $T^\pm$. We note that the periodic orbits satisfy the BVP:

$$\begin{aligned}\dot{x}^\pm - f(x^\pm,\alpha) &= 0 \\ x^\pm(0) - x^\pm(T^\pm) &= 0\end{aligned}$$

We can non-dimensionalize this BVP to get:

$$\begin{aligned}\dot{x}^\pm - Tf(x^\pm,\alpha) &= 0 \\ x^\pm(0) - x^\pm(1) &= 0\end{aligned} \tag{4.2.1}$$

Let $M^\pm$ be the monodromy matrices of $x^\pm(t)$ starting at $x^\pm(0)$ respectively. Define $N^\pm$ analogously as the adjoint monodromy matrices of $x^\pm(t)$ starting at $x^\pm(0)$ respectively. Suppose also that $M^\pm$ both have at least one stable Floquet multiplier. Then $x^\pm(t)$ are called limit cycles of (4.1.1).

We will associate the notation $O^{\pm}$ with the limit cycles $x^{\pm}(t)$ respectively. Define W^s_+, W^u_+ as the stable and unstable invariant manifolds of the cycle O^+. Define W^s_- and W^u_- as the stable and unstable invariant manifolds of O^-. A connecting orbit from O^- to O^+, call it $u(t)$, is a solution of (4.1.1) if it satisfies:

$$\lim_{t\to\pm\infty} dist\left(u(t), O^{\pm}\right) = 0 \tag{4.2.2}$$

Where *dist* is the least euclidean distance between the solution u at a given time and the periodic orbit. The two periodic orbits and the connecting orbit can be represented by a system of ODEs and some boundary conditions.

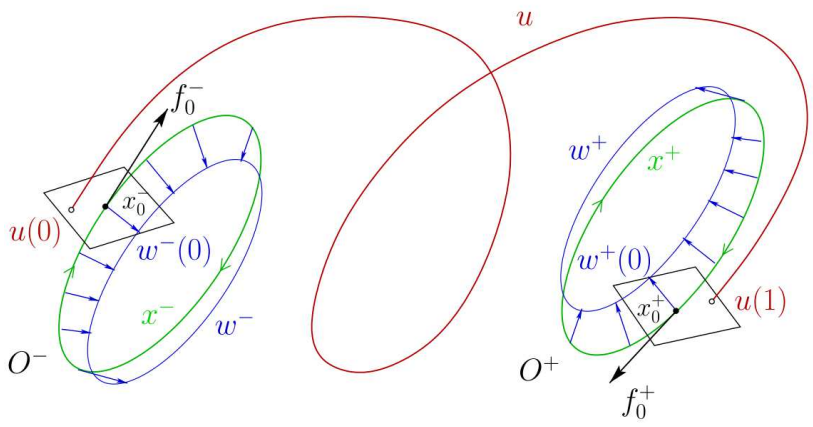

Figure 4.1: Heteroclinic orbit of limit cycles. The picture is from [7].

An algorithm for parameter continuation of such a system with two periodic orbits and a connecting orbit is the subject of [7]. The case $dim(W^u_-) = 2 = dim(W^s_+)$ in a phase space of dimension 3, is contained therein. Here we modify the algorithm to deal with the case $dim(W^u_-) = 2$ and $dim(W^s_+) = n - 1$ in an n dimensional phase space. That is we still require that both limit cycles must have precisely one unstable Floquet multiplier, however the dimension of the phase space may vary. We now set up the BVP following the text of [7] closely with slight modifications.

Let M be a monodromy matrix with associated period T. Suppose that ν is a

solution to (4.1.2) such that $\nu(0) \neq 0$ and $M\nu = \mu\nu$. Then by definition $\nu(T) = M\nu(0) = \mu\nu(0)$. The non-dimensionalized, normalized ν must satisfy the following BVP:

$$\begin{aligned} \dot{\nu} - TJ(t)\nu &= 0 \\ \nu(1) - \mu\nu(0) &= 0 \\ \langle \nu(0), \nu(0) \rangle - 1 &= 0 \end{aligned}$$

Assuming that $\nu(0) > 0$, $\exists \omega(t)$ such that:

$$\mu = e^{\lambda} \quad , \quad \nu(t) = e^{\lambda}\omega(t)$$

Then ω will satisfy the following BVP:

$$\begin{aligned} \dot{\omega} - TJ(t)\omega + \lambda\omega &= 0 \\ \omega(1) - \omega(0) &= 0 \\ \langle \omega(0), \omega(0) \rangle - 1 &= 0 \end{aligned} \tag{4.2.3}$$

The BVP given by (4.2.3) is more stable than its predecessor [7] and hence we will be using it for calculations.

Suppose we had instead started with an adjoint monodromy matrix, N, with associated period T. Suppose also that, $\nu(t)$, is a solution of (4.1.3) with $N\nu(0) = \mu\nu$ and $mu > 0$. We have $\nu(T) = \mu\nu(0)$. Set:

$$\nu = e^{\lambda} \quad , \quad \nu(t) = e^{\lambda}\omega(t)$$

By a similar argument as above we can show that ω must satisfy the following boundary value problem:

$$\begin{aligned} \dot{\omega} + TJ^{\dagger}(t)\omega + \lambda\omega &= 0 \\ \omega(1) - \omega(0) &= 0 \\ \langle \omega(0), \omega(0) \rangle - 1 &= 0 \end{aligned} \tag{4.2.4}$$

Now suppose μ^{+} is the sole unstable Floquet multiplier of M^{+}. We know there

exists exactly one stable Floquet multiplier of N^+, μ^+, and an associated stable eigenvector ω^+. By the above discussion of eigenvectors of the adjoint monodromy matrix we know that ω^+ will be orthogonal to W^s_+. Suppose also that μ^-, ω^- are the sole unstable Floquet multiplier and eigenvector of M^- respectively. Set $\lambda^\pm = ln(\mu^\pm)$.

The BVP as required by us is then given by the following equations.

1. The equations describing the periodic orbit:

$$\begin{aligned} \dot{x}^\pm - T^\pm f(x^\pm, \alpha) &= 0 \\ x^\pm(0) - x^\pm(1) &= 0 \end{aligned} \tag{4.2.5}$$

2. The equations describing the direction of arrival at O^+ orbit:

$$\begin{aligned} \dot{\omega}^+ + T^+ J^\dagger(t)\omega^+ + \lambda^+\omega^+ &= 0 \\ \omega^+(1) - \omega^+(0) &= 0 \\ \langle \omega^+(0), \omega^+(0) \rangle - 1 &= 0 \end{aligned} \tag{4.2.6}$$

3. The equations describing the direction of departure at O^- orbit:

$$\begin{aligned} \dot{\omega}^- - T^- J(t)\omega^- + \lambda^-\omega^- &= 0 \\ \omega^-(1) - \omega^-(0) &= 0 \\ \langle \omega^-(0), \omega^-(0) \rangle - 1 &= 0 \end{aligned} \tag{4.2.7}$$

4. The equations describing the connecting orbit:

$$\begin{aligned} \dot{u} - T f(u, \alpha) &= 0 \\ \langle f(x^+(0), \alpha), u(1) - x^+(0) \rangle &= 0 \\ \langle \omega^+(0), u(1) - x^+(0) \rangle &= 0 \\ u(0) - x^-(0) - \epsilon\omega^-(0) &= 0 \end{aligned} \tag{4.2.8}$$

5. A phase condition for each of the cycles

$$\Phi\left[x^{\pm}\right] = 0 \tag{4.2.9}$$

The phase condition Φ fixes the base point $x^{\pm}(0)$ on each of the respective cycles $O^{\pm}$. For example, we may set:

$$\Phi\left[x^{+}\right] = x_j^{+}(0) - a_j$$

so that we fix the base point by the use of a specified coordinate value a_j for a given parameter value.

The total number of unknowns is 92 which are found in $x^{\pm}(0), \omega^{\pm}(0), u(0), T^{\pm}, \lambda^{\pm}, \epsilon, T$ and one system parameter. These unknowns must satisfy 89 boundary conditions described above. Finally there two integral conditions which the unknowns must satisfy given by (4.2.9). This gives us 92 unknowns and 91 equations. Therefore we can use arclength continuation to solve for a 1-parameter family of solutions given an initial solution.

Conclusions and Outlook

In Chapter 1 we introduced the onset of turbulence in PCF, TCF and other geometries. The seeming contradiction between the instability of the laminar profile of PCF in laboratory settings and the stability of it predicted by theory was discussed. The work of Nagata, Kida & Kawahara and Waleffe in reconciling these two facts through the discovery of numerical non-laminar periodic solutions and the SSP was discussed. Heteroclinic and homoclinic orbits of periodic solutions play a crucial role in the onset of turbulence for PCF where the laminar profile is linearly stable. We discussed also Waleffe's low-order model of PCF and its significance to the SSP. We emphasized the relevance of this low order model to PCF itself. The seed from which this thesis grew was the periodic solution found by van Veen [20] for an extended Waleffe model (EWM) of PCF through the use of a method analogous to Nagata's and the bifurcation analysis of that periodic solution. The results of this bifurcation analysis are shown in Section 2.4. Here we summarize them:

- We used MatCont to calculate the bifurcation diagram of the periodic solution of EWM found by van Veen.
- We detected curves of LPC and NS bifurcations.
- We detected two LPNS bifurcation. These are co-dimension 2 bifurcations with 4D center manifolds.

In Chapter 2 we introduced bifurcation theory and the use of normal forms and the central manifolds to study the dynamics of periodic solutions near bifurcation points. Specifically we used de Witte's recent calculation of the normal form for the LPNS bifurcation to predict the dynamics of the periodic solution of EWM discussed above near the LPNS point. In order to numerically explore these dynamics, in Chapter 3

we applied the unstable manifold computation method introduced in [21]. The results of that analysis are shown in Section 2.4 and Section 3.1. We summarize those results here:

- We found an isola of periodic orbits near one of the LPNS bifurcations.
- We isolated the periodic orbits in that isola which had precisely one unstable multiplier.
- Through a crude shooting method we identified some periodic solutions near which interesting dynamics occured.
- Using the unstable manifold computation technique we explored the unstable manifolds of the identified periodic orbits.
- We found homoclinic orbits of periodic solutions in the EWM.
- We found quasi-periodic orbits of the EWM.

In Chapter 4 we modified a method, described in [7], to refine and continue a homoclinic or heteroclinic orbit of periodic solutions. We hope to implement this method starting with an initial homoclinic orbit, such as the one described in Section 3.1. Further we want to find a heteroclinic orbit by expanding our search using the unstable manifold computation.

We want to explore the region, in parameter space, in which these homoclinic and heteroclinic orbits exist for the EWM. The importance of heteroclinic and homoclinic orbits in the onset of turbulence in PCF were discussed in Section 1.5.1. Although heteroclinic orbits have been found for PCF at this point it is very difficult to continue them through a BVP problem. This is because a key step in the method described in 4 is the computation of the adjoint variational problem. The computation of the adjoint variational problem for PCF has not yet been perfromed. Instead of PCF, we have isolated homoclinic orbits in the EWM. Here the computation of the adjoint variational problem is feasible and thus a continuation of the homoclininc orbit is

feasible as well. The low-order model that we use has many of the properties of PCF. For example, the linear laminar profile is stable and we can find a periodic solution that we can continue to $Re \to \infty$. The exploration of the region in which homoclinic and heteroclinic orbits exist for the EWM will be a small step in understanding the nature of homoclinic and heteroclinic orbits in PCF.

Bibliography

[1] D.J. Acheson. *Elementary Fluid Dynamics*. Oxford Applied Mathematics and Computing Science Series. Clarendon Press, 1995.

[2] J. Baggett and L. Trefethen. Low-Dimensional Models of Subcritical Transition to Turbulence. *Phys. Fluids*, 261:578–584, 1993.

[3] Wikimedia Commons. The Great Wave off Kanagawa. http://upload.wikimedia.org/wikipedia/commons/thumb/0/0d/Great_Wave_off_Kanagawa2.jpg/1280px-Great_Wave_off_Kanagawa2.jpg, 1833. Accessed: 2015-01-09.

[4] V. De Witte. *Computational Analysis of Bifurcations of Periodic Orbits*. PhD thesis, Ghent University, 2013.

[5] A. Dhooge, W. Govaerts, and Y.A. Kuznetsov. MATCONT: A MATLAB Package For Numerical Bifurcation Analysis of ODEs. *ACM. T. Math. Software*, 29(2):141–164, 2003.

[6] E. Doedel, Y. Kuznetsov, B. Kooi, and Van Voorn G. Continuation of Connecting Orbits in 3D-ODEs: (i) Point-To-Cycle Connections. *Int. J. Bifurcat. Chaos*, 18:1889–1905, 2008.

[7] E. Doedel, Y. Kuznetsov, B. Kooi, and Van Voorn G. Continuation of Connecting Orbits in 3D-ODEs: (ii) Cycle-To-Cycle Connections. *Int. J. Bifurcat. Chaos*, 19:159–169, 2009.

[8] E. J. Doedel, A. R. Champneys, F. Dercole, T. F. Fairgrieve, Yu. A. Kuznetsov, B. Oldeman, R. Paffenroth, B. Sandstede, X. Wang, and C. Zhang.

AUTO-07P: Continuation and Bifurcation Software for Ordinary Differential Equations, 2008. Concordia University, Montreal, Canada. Available from http://sourceforge.net/projects/auto-07p/.

[9] J. M. Hamilton, J. Kim, and F. Waleffe. Regeneration Mechanisms of Near-Wall Turbulence Structures. *J. Fluid. Mech.*, 287:317–348, 1995.

[10] Clay Mathematical Institute. Navier-stokes equation. http://www.claymath.org/millenium-problems/navier%E2%80%93stokes-equation. Accessed: 2015-01-09.

[11] G. Kawahara and K. Kida. Periodic Motion Embedded in Plane Couette Turbulence: Regeneration Cycle and Burst. *J. Fluid. Mech.*, 449:291–300, 2001.

[12] G. Kawahara, S. Kida, and L. van Veen. Unstable Periodic Motion in Turbulent Flows. *Nonlinear Proc. Geoph.*, 13:499–507, 2006.

[13] G. Kawahara, M. Uhlmann, and L. van Veen. The Significance of Simple Invariant Solutions in Turbulent Flows. *Annu. Rev. Fluid. Mech.*, 44:203–225, 2012.

[14] Y. Kuznetsov, H. Meijer, and L. van Veen. The Fold-Flip Bifurcation. *Int. J. Bifurcat. Chaos*, 14:2253–2282, 2004.

[15] Y.A. Kuznetsov. *Elements of Applied Bifurcation Theory*, volume 112. Springer Verlag, 1998.

[16] M. Nagata. Three-Dimensional Finite-Amplitude Solutions in Plane Couette Flow: Bifurcation From Infinity. *J. Fluid. Mech.*, 217:519–527, 1990.

[17] V.A. Romanov. Stability of Plane-Parallel Couette Flow. *Funct. Anal. Appl+*, 7:62–73, 1973.

[18] B. Saltzman. Finite Amplitude Free Convection as an Initial Value Problem .i. *J. Atmos. Sci.*, 19:329–342, 1962.

[19] L. Trefethen, A. Trefethen, S. Reddy, and Driscoll. T. Hydrodynamic Stability without Eigenvalues. *Science*, 261:578–584, 1993.

[20] L. van Veen. Unstable Periodic Orbits in Turbulence, in *proceedings of the fifth euromech nonlinear dynamics conference. ENOC5*, 2005.

[21] L. Van Veen, G. Kawahara, and S. Kida. On Matrix-Free Computation of 2D Unstable Manifolds. *SIAM J. Sci. Comput.*, 33:25–44, 2011.

[22] D. Viswanath. Recurrent Motions Within Plane Couette Turbulence. *J. Fluid. Mech.*, 580:339–358, 2007.

[23] R. Vitolo, H.W. Broer, and C. Simó. Routes to Chaos in the Hopf-Saddle-Node Bifurcation for Fixed Points of 3D-Diffeomorphisms. *Nonlinearity*, 23:1919–2010, 2010.

[24] F. Waleffe. Transition in Shear Flows: Non-Linear Normality versus Non-Normal Linearity. *Phys. Fluids*, 7:3060–3066, 1995.

[25] F. Waleffe. On a Self-Sustaining Process in Shear Flows. *Phys. Fluids*, 9:883–900, 1997.

[26] F. Waleffe. Shear Turbulence: Onset and Structure, in *proceedings of the 2011 program in geophysical fluid dynamics*. https://www.whoi.edu/main//gfd/proceedings-volumes/2011, 2011. Accessed: 2013-06-01.

[27] S. Wiggins. *Introduction to Applied Nonlinear Dynamical Systems and Chaos*. Texts in Applied Mathematics 2. Springer-Verlag, 1990.